
DEEP HYBRID MODELS: INFER AND PLAN IN THE REAL WORLD

Matteo Priorelli

Institute of Cognitive Sciences and Technologies
National Research Council of Italy
Padova, Italy
matteo.priorelli@gmail.com

Ivilin Peev Stoianov

Institute of Cognitive Sciences and Technologies
National Research Council of Italy
Padova, Italy
ivilinpeev.stoianov@cnr.it

ABSTRACT

Determining an optimal plan to accomplish a goal is a hard problem in realistic scenarios, which often comprise dynamic and causal relationships between several entities. Although traditionally such problems have been tackled with optimal control and reinforcement learning, a recent biologically-motivated proposal casts planning and control as an inference process. Among these new approaches, one is particularly promising: *active inference*. This new paradigm assumes that action and perception are two complementary aspects of life whereby the role of the former is to fulfill the predictions inferred by the latter. In this study, we present an effective solution, based on active inference, to complex control tasks. The proposed architecture exploits hybrid (discrete and continuous) processing to construct a hierarchical and dynamic representation of the self and the environment, which is then used to produce a flexible plan consisting of subgoals at different temporal scales. We evaluate this *deep hybrid model* on a non-trivial task: reaching a moving object after having picked a moving tool. This study extends past work on planning as inference and advances an alternative direction to optimal control and reinforcement learning.

1 Introduction

State-of-the-art solutions to tackle complex control tasks generally rely on deep Reinforcement Learning (RL) [1, 2]. While this approach has led to remarkable advances in machine learning, neural networks have well-known issues regarding data efficiency, explainability, and generalization [3]. Instead, the human brain is capable of learning novel tasks with a small amount of samples, transferring the knowledge previously acquired in similar situations. A recent hypothesis on how this is possible is called the *Bayesian brain*, which proposes that the brain makes sense of the world by constructing a hierarchical generative model that constantly makes predictions and tests hypotheses over its percepts [4]. The theory of predictive coding [5, 6] is based on this assumption and, while having its roots in data compression [7], has led to a biologically-inspired alternative to traditional deep learning in the form of *Predictive Coding Networks* (PCNs). Such networks have been shown to generalize well to classification or regression tasks [8, 9], while being a reasonable approximation of backprop [10, 11, 12, 13]. However, few studies used the modular and hierarchical nature of predictive coding to represent the model dynamics and interact with the environment [14, 15, 16, 17, 18, 19], mostly done through RL.

An additional concern about RL has been raised in recent years: expressing goals in terms of value functions may not be as biologically plausible as previously thought, since many cases have been observed where dopamine (the putative responsible for rewards and punishments) does not appear to transmit reward prediction errors, e.g., when considering aversive stimuli [20, 21]; crucially, from a machine learning perspective, it might limit the range of motions that an agent can learn [22]. Instead, complex movements such as handwriting or walking can be easily realized by a generative model encoding goals as prior beliefs over the environment [23]. The theory of active inference builds upon this premise: it postulates that goal-directed behavior is the result of a biased representation of the world, generating a cascade of prediction errors that ultimately leads the agent to sample those observations that make its beliefs true [24, 25, 26, 27]. In this view, the tradeoff between exploration and exploitation arises naturally, driving the agent to minimize the uncertainty of its internal model before maximizing potential rewards [28].

This perspective might be key for advancing with current machine learning and, in particular, with a research area that characterizes control and planning as an inference process [29, 30, 31, 32]. A distinctive feature of active inference is that one can model the environment via a hierarchy of causes and dynamic states unfolding at different timescales [33], fundamental, e.g., for linguistic communication [34]. At present, however, hierarchical models in active inference have not been studied in depth compared to predictive coding, and adaptation to complex data still relies on using neural networks as generative models [35, 36, 37, 38, 39, 40, 41, 42, 43]. One study showed that a deep hierarchical agent with independent dynamics functions for each level can constantly modify its internal trajectories to match prior expectations, affording advanced control of complex kinematic chains [44]. Hence, the possibility of expressing and learning intermediate timescales could bring many advantages to solving standard RL tasks. When modeling the real world, active inference makes use of so-called *hybrid* or *mixed models*, combining discrete decision-making with continuous motions. However, state-of-the-art applications have used hybrid models only in static contexts [26, 45, 46, 47, 48], and operating in dynamic environments requires additional frameworks [42].

In this work, we address these issues from a unified perspective. Our contributions are briefly summarized as follows:

- We present an active inference agent affording robust planning in changing environments. This agent comprises several units that dynamically infer the state of affairs of the world, and a high-level discrete model that synchronizes their behavior and plans composite movements.
- We then consider a modular architecture for tasks requiring deep hierarchical modeling, e.g., tool use. Its connectivity resembles PCNs or traditional neural networks, and is a first step toward designing deep structures in active inference that can generalize over (and learn) novel tasks.
- Finally, we investigate the agent’s behavior under a non-trivial task, i.e., reaching a moving ball after reaching and picking a moving tool. We show the interactions between the agent’s intentions, and the dynamic accumulation of sensory evidence. With the proposed approach, the agent is able to infer and plan in changing environments and via flexible hierarchies.

2 Results

2.1 Deep hybrid modeling

Analyzing the emergence of distributed intelligence, [49] emphasized three kinds of depth within the framework of active inference: factorial, temporal, and hierarchical. Factorial depth implies the existence of independent factors in the agent’s generative model (e.g., objects of an environment or more abstract states), which can be combined to generate outcomes and transitions. Temporal depth entails, in discrete terms, a vision into the imminent future that can be used for decision-making; or, in continuous terms, increasingly precise estimates of dynamic trajectories needed, for instance, in generating smooth movements. Hierarchical depth introduces spatial causal relationships between different levels, inducing a separation of temporal scales whereby higher levels happen to construct more invariant representations, while lower levels can better capture the rapid changes of sensory stimuli.

In the following, we present the main features of a *deep hybrid model*, describing factorial, temporal, and hierarchical depths in the contexts of flexible behavior, dynamic planning, and iterative transformations of reference frames. By deep hybrid model, we intend an active inference model composed of hybrid units connected hierarchically. Here, hybrid means that discrete and continuous representations are encoded within each unit, wherein the communication between the two is achieved by Bayesian model reduction [50, 51]. All the internal operations can be computed through automatic differentiation, i.e., by maintaining the gradient graph when performing each forward pass and propagating back the prediction errors. For a detailed treatment of predictive coding, hierarchical active inference in discrete and continuous state-spaces, and Bayesian model comparison, see Appendices A, B, and C.

2.1.1 Factorial depth and flexible behavior

Figure 1 depicts the factor graph of a *hybrid unit* \mathcal{U} . The variables are: continuous hidden states \mathbf{x} and \mathbf{x}' , observations \mathbf{y} , and discrete hidden causes \mathbf{v} . The hidden states comprise two temporal orders, and the first component will be indicated as the 0th order. The factors are: dynamics functions \mathbf{f} , and likelihood functions \mathbf{g} . Note also a prior over the 0th-order hidden states $\mathbf{\eta}$, and a prior over the hidden causes \mathbf{H} encoding the agent’s goals. The generative model is the

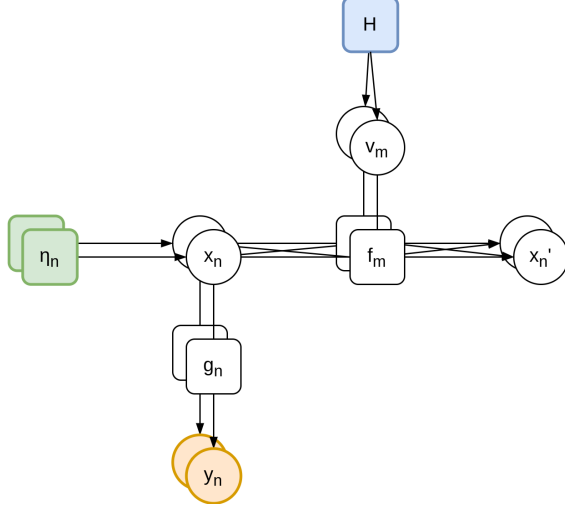


Figure 1: Factor graph of a hybrid unit. Continuous hidden states \mathbf{x} generate predictions \mathbf{y} through parallel pathways. The model dynamics is encoded in functions f_m , which are hypotheses of how the world may evolve and are associated with discrete hidden causes \mathbf{v} .

following:

$$p(\mathbf{x}, \mathbf{x}', \mathbf{v}, \mathbf{y}) = p(\mathbf{y}|\mathbf{x})p(\mathbf{x}'|\mathbf{x})p(\mathbf{x})p(\mathbf{v}) \quad (1)$$

We assume that hidden causes and hidden states have different dimensions, resulting in two factorizations. The hidden states, with dimension N , are sampled from independent Gaussian distributions and generate predictions in parallel pathways:

$$p(\mathbf{x}) = \prod_n^N \mathcal{N}(\boldsymbol{\eta}_n, \boldsymbol{\Sigma}_{\eta,n}) \quad p(\mathbf{y}|\mathbf{x}) = \prod_n^N \mathcal{N}(\mathbf{g}_n(\mathbf{x}_n), \boldsymbol{\Sigma}_{y,n}) \quad (2)$$

where $\boldsymbol{\Sigma}_{\eta,n}$ and $\boldsymbol{\Sigma}_{y,n}$ are their covariance matrices. The hidden causes, with dimension M , are instead sampled from a categorical distribution:

$$p(\mathbf{v}) = \text{Cat}(\mathbf{H}) \quad (3)$$

This differs from state-of-the-art hybrid architectures which assume separate continuous and discrete models with continuous hidden causes (see Appendix B) [52]. A discrete hidden cause v_m concurs, with hidden states \mathbf{x} , in generating a specific prediction for the 1st temporal order \mathbf{x}' :

$$p(\mathbf{x}'|\mathbf{x}, m) = \mathcal{N}(\mathbf{f}_m(\mathbf{x}), \boldsymbol{\Sigma}_{x,m}) \quad (4)$$

This probability distribution entails a hypothetical evolution of the hidden states, which the agent maintains to infer the real state of affairs of the world and move. More formally, we consider $p(\mathbf{x}'|\mathbf{x}, m)$ as being the m th reduced version of a full model:

$$p(\mathbf{x}'|\mathbf{x}) = \mathcal{N}(\boldsymbol{\eta}'_x, \boldsymbol{\Sigma}_x) \quad (5)$$

This allows us – using the variational approach for approximating the true posterior distributions – to convert discrete into continuous signals and vice versa through Bayesian model averaging and Bayesian model comparison, respectively (see Appendix C and [50, 51]). In particular, top-down messages combine the potential trajectories $\mathbf{f}_m(\mathbf{x})$ with the related probabilities encoded in the discrete hidden causes v_m :

$$\boldsymbol{\eta}'_x = \sum_m v_m \mathbf{f}_m(\mathbf{x}) \quad (6)$$

This computes a dynamic path that is an average of the agent’s hypotheses, based on its goals. Conversely, bottom-up messages compare the agent’s prior surprise $-\log \mathbf{H}$ with the log evidence l_m of every reduced model. The latter is

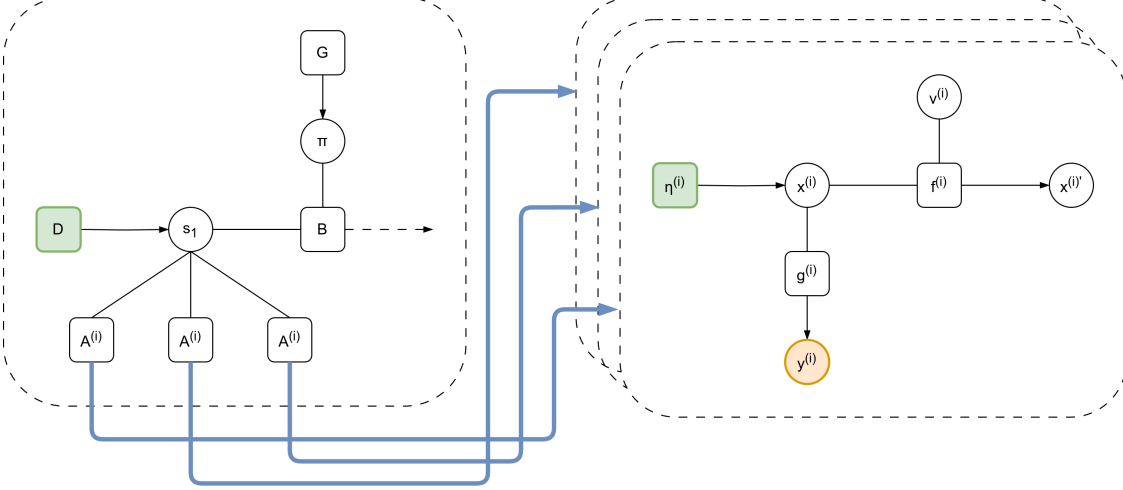


Figure 2: Interface between a discrete model and several hybrid units. The hidden causes $v^{(i)}$ are directly generated, in parallel pathways, from discrete hidden states s_τ via likelihood matrices $A^{(i)}$.

accumulated over a continuous time T :

$$l_m = \int_0^T \frac{1}{2} (\mu_m'^T P_{x,m} \mu_m' - f_m(x)^T \Pi_{x,m} f_m(x) - \mu'^T P_x \mu' + \eta_x'^T \Pi_x \eta_x') dt \quad (7)$$

where μ_m , $P_{x,m}$, and $\Pi_{x,m}$ are the mean, posterior precision, and prior precision of the m th reduced model. In this way, the agent builds a discrete world representation by inferring – within the same discrete period τ – which dynamic hypothesis is most likely to have generated the current perceptions – see [53] for more details about this approach.

Furthermore, a single hybrid unit has useful features that derive from the factorial depths of hidden states and causes. Consider the case where the hidden states encode the agent’s configuration and other environmental objects, while the hidden causes represent the agent’s intentions. A hybrid unit could dynamically assign the causes of its actions at a particular moment: this is critical, e.g., in a pick and place operation, during which an object is first the cause of the hand movements¹ – resulting in a picking action – but then it is the consequence of another cause (i.e., a goal position) – resulting in a placing action. This approach differs from other solutions [55, 24] that directly encode a target location in the hidden causes. Further, encoding environmental entities – and not just the self – into the hidden states permits inferring their dynamic trajectories, which is fundamental, e.g., in catching objects on the fly [56] or in tracking a hidden target with the eyes [57].

2.1.2 Temporal depth and dynamic planning

Consider the following discrete generative model:

$$p(s_{1:\tau}, o_{1:\tau}, \pi) = p(s_1) p(\pi) \prod_{\tau} p(o_{\tau} | s_{\tau}) p(s_{\tau} | s_{\tau-1}, \pi) \quad (8)$$

where:

$$\begin{aligned} p(s_1) &= \text{Cat}(\mathbf{D}) & p(o_{\tau} | s_{\tau}) &= \text{Cat}(\mathbf{A}) \\ p(\pi) &= \sigma(-\mathcal{G}) & p(s_{\tau+1} | s_{\tau}, \pi) &= \text{Cat}(\mathbf{B}_{\pi, \tau}) \end{aligned} \quad (9)$$

Here, \mathbf{A} , \mathbf{B} , \mathbf{D} are the likelihood matrix, transition matrix, and prior, π is the policy, s_{τ} are the discrete hidden states at time τ , o_{τ} are the discrete observations, and \mathcal{G} is the *expected free energy* (see Appendix B for more details).

¹In active inference, it is a limb (extrinsic) trajectory that produces (intrinsic) muscle movements; see Appendix B and [23, 54] for a more detailed treatment.

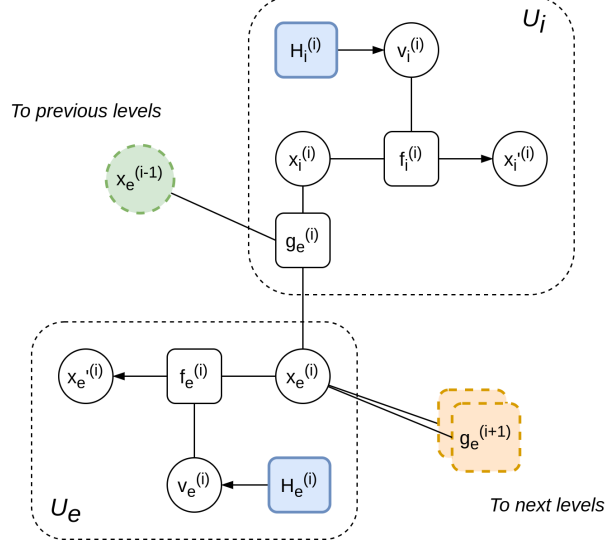


Figure 3: A signal $x_e^{(i)}$ in an extrinsic reference frame is iteratively transformed. Different IE modules can be combined in a multiple-output system.

We can let the discrete likelihood $p(o_\tau | s_\tau)$ directly bias the discrete hidden causes of a hybrid unit:

$$H_\tau \equiv As_\tau \quad o_\tau \equiv v_\tau \quad (10)$$

This is an alternative method to the state-of-the-art, which considers an additional level between discrete observations and static priors over continuous hidden causes [45]. With this approach, the discrete model can impose discrete priors that unfold into dynamic trajectories even in the same period τ , thus affording dynamic planning [53, 58]. If a discrete model is then linked to different hybrid units in parallel – as shown in Figure 2 – the discrete hidden states are inferred by combining multiple evidences:

$$s_{\pi,\tau} = \sigma(\ln B_{\pi,\tau-1} s_{\pi,\tau-1} + B_{\pi,\tau+1}^T s_{\pi,\tau+1} + \sum_n \ln A^{(i)T} v_\tau^{(i)}) \quad (11)$$

where $s_{\pi,\tau}$ are the discrete hidden states conditioned over policy π at time τ , while the superscript i indicates the i th hybrid unit. These parallel pathways synchronize the behavior of all low-level units based on the same high-level plan, allowing, e.g., simultaneous coordination of every limb. In Figure 2, we notice the two temporal depths peculiar to active inference. One lets an agent make plans by accumulating the expected free energy in a time horizon defined by the policy length [59]. The second temporal depth refines dynamic trajectories with increasing frequency, and can be used to infer more accurately the discrete variables.

2.1.3 Hierarchical depth and iterative transformations

Equation 11 introduces a hierarchical dependency wherein a high-level discrete model imposes priors over low-level hybrid units. Hierarchical depth is critical in many tasks that require learning of modular and flexible functions. Considering motor control, forward kinematics is repeated throughout every element of the kinematic chain, computing the end effector position from the body-centered reference frame. Iterative transformations are also fundamental in computer vision, where camera models perform roto-translations and perspective projections in sequence. How can we express such hierarchical computations in terms of inference? We design a structure called *Intrinsic-Extrinsic* (or IE) module, performing iterative transformations between reference frames [44, 60]. A unit \mathcal{U}_e encodes a signal in an extrinsic reference frame, while another unit \mathcal{U}_i represents an intrinsic signal. A likelihood function $g_e^{(i)}$ applies a transformation to the extrinsic signal based on the intrinsic information, and returns a new extrinsic state:

$$g_e^{(i)}(x_i^{(i)}, x_e^{(i-1)}) = T^{(i)}(x_i^{(i)}) \cdot x_e^{(i-1)} \quad (12)$$

where $\mathbf{T}^{(i)}$ is a linear transformation matrix. This new state can then act as a prior for the subordinate levels in a multiple-output system; indicating with the superscript (i, j) the i th hierarchical level and the j th unit within the same level, we link the IE modules in the following way:

$$\mathbf{y}_e^{(i,j)} \equiv \mathbf{x}_e^{(i+1,j)} \quad \mathbf{x}_e^{(i-1,j)} \equiv \boldsymbol{\eta}_e^{(i,j)} \quad (13)$$

as displayed in Figure 3. Ill-posed problems that generally have multiple solutions – such as inverse kinematics or depth estimation – can be solved by inverting the agent’s generative model and backpropagating the sensory prediction errors, with two additional features compared to traditional methods: (i) the possibility of steering the optimization by imposing appropriate priors, e.g., for avoiding singularities during inverse kinematics; (ii) the possibility of acting over the environment to minimize uncertainty, e.g., with motion parallax during depth estimation.

Encoding signals in intrinsic and extrinsic reference frames also induces a decomposition over dynamics functions, leading to simpler (and yet richer) attractor states. This is useful for tasks requiring multiple constraints in both domains, e.g., when walking with a glass in hand [44]. Further, the factorial depth previously described allows us to represent hierarchically not only the self, but also the objects in relation to the self, along with the kinematic chains of other agents [58]. In this way, an agent could maintain a potential representation of itself whenever it observes a relevant entity; this representation can then be realized efficiently as soon as necessary. Furthermore, the complete deep hybrid model presents two different temporal scales: (i) a discrete scale that separates the slow-varying representation of the task with the fast update of continuous signals; (ii) a continuous scale in which the prediction errors coming from the last levels of the hierarchy (e.g., the limbs) have a minor impact as they flow back to the first levels (e.g., the body-centered reference frame).

2.2 A deep hybrid model for flexible tool use

In this section, we show how a deep hybrid model can be used efficiently in a task that requires planning in a dynamic environment and coordination of multiple elements of the agent’s body. The implementation details are found in Appendix D, while Appendix E illustrates the algorithms for the inference of the discrete model and hybrid units. Then, we analyze the task and describe the effects of dynamic planning in terms of accumulated sensory evidence and transitions over discrete hidden states.

Reaching an object with a tool is a complex task that requires all the features delineated in the previous section. First, the task has to be decomposed into two subgoals – reaching the tool and reaching the object – so it requires a discrete model that can perform high-level planning. Second, the agent has to maintain distinct beliefs about its arm, the tool, and the object, which must be inferred from sensory observations if the environment changes. Third, if the tool has to be grasped at the origin while the object has to be reached with its extremity, the agent’s generative model should encode a hierarchical representation of every entity, and goals in the form of attractors should be imposed at different levels.

As displayed in the virtual environment of Figure 4a, the agent controls an arm of 4 Degrees of Freedom (DoF). It has access to proprioceptive information about its joint angles, and exteroceptive (e.g., visual) observations about the positions of its limbs, the tool, and the ball. For simplicity, we assume that the tool sticks to the agent’s end effector as soon as it is touched.² The generative model is composed of as many IE modules as the agent’s DoF, following the hierarchical causal relations of the forward kinematics. Each module is then factorized into three independent components representing the arm and the two objects, which will be indicated with the subscripts a , t , and b . Together, these characteristics provide an effective decomposition into three parallel pathways: one maintaining an estimate of the agent’s current configuration (both in terms of joint angles and limb positions), and other two representing potential agent’s configurations in relation to the objects. The message passing of *extrinsic prediction errors*, i.e., differences between the estimated limb positions and their predictions made by the estimated joint angles, allows to infer the whole body configuration (either real or potential) via exteroceptive observations. In addition, every component of a level exchanges lateral messages with the other components, in the form of *dynamics prediction errors*. These errors are caused by the dynamics functions which define the interactions between entities.

There are two crucial aspects arising when modeling entities in a deep hierarchical fashion and related to the self. First, different configurations could be inferred (hence, different movements) depending on the hierarchical location of the object considered – e.g., reaching a ball with either the elbow or the end effector. Second, entities could have their

²For a more realistic grasping simulation, see [53, 56]

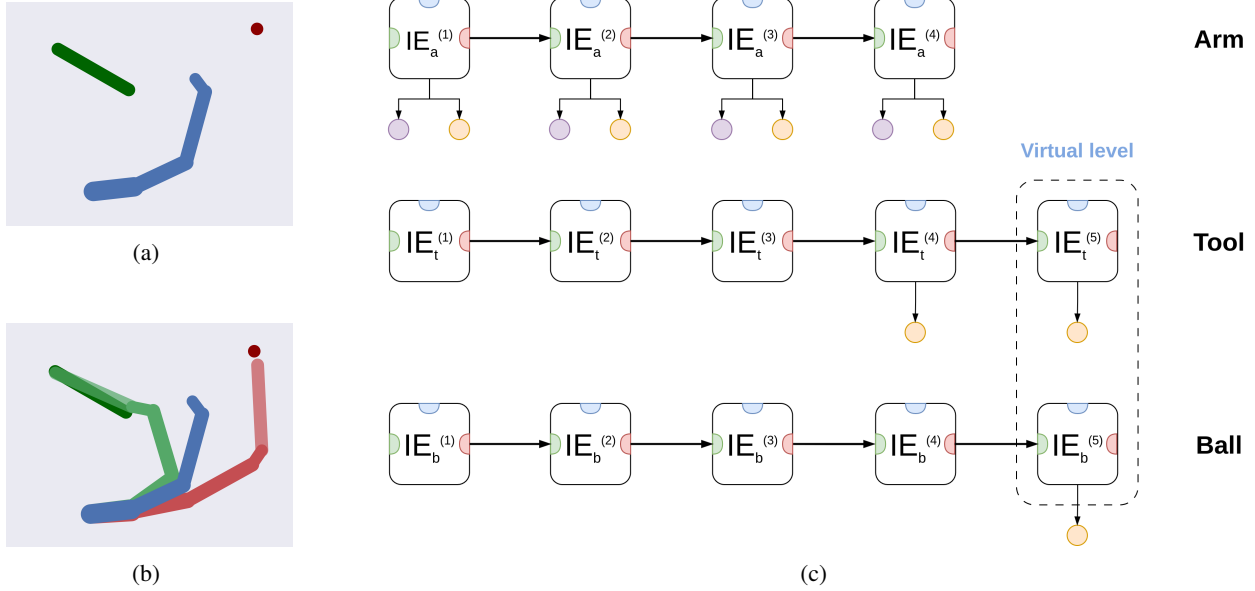


Figure 4: (a) Virtual environment of the tool use task. An agent controlling a 4-DoF arm has to grasp a moving tool (in green) and reach a moving ball (in red) with the tool’s extremity. (b) Agent’s beliefs over the hidden states of the arm (blue), tool (light green), and ball (light red). The real positions of the tool and ball are represented in dark green and dark red, respectively. The virtual levels are plotted with more transparent colors. (c) Graphical representation of the agent’s generative model. Every environmental entity is encoded hierarchically by considering the whole arm’s kinematic structure. For clarity, the three pathways are displayed separately, while lateral connections and the high-level discrete model are not shown. The tool and the ball are augmented with an additional virtual level representing a new joint. Small purple and yellow circles represent proprioceptive and exteroceptive observations, respectively.

own hierarchical structures: in our application, the tool consists of two Cartesian positions and an angle, and the agent should somehow represent this additional link if it wants to interact with the tool’s origin and extremity. For these reasons, we consider a virtual level for the tool component, attached to the last (end effector) level, as exemplified in Figure 4c; the visual observations of the tool are then linked to the last two levels. From these observations, the correct tool angle can be inferred as if it were a new joint angle of the arm. Additionally, since we want the agent to touch the ball with the tool’s extremity, we model the third component of the hidden states with a similar deep hierarchical structure, in which a visual observation of the ball is attached to the last virtual level. The overall architecture can be better understood from Figure 4b, showing the agent’s beliefs of all three entities. As soon as the agent perceives the tool, it infers a possible kinematic configuration as if it had only visual access to its last two joints. Likewise, perceiving the ball causes the agent to find an extended kinematic configuration as if the tool were part of the arm.

At this point, specifying the correct dynamics for goal-directed behavior is simple. We first define two sets of dynamics functions, one for reaching the tool and another for reaching the ball with the tool’s extremity. As explained in Appendix D, the second step requires an attractor at the virtual level, letting the agent think that the tool’s extremity will be pulled toward the ball. This biased state generates an extrinsic prediction error that is backpropagated to the previous level encoding the tool’s origin and the end effector. Finally, defining discrete hidden states and discrete hidden causes related to the agent’s intentions allows the agent to accumulate evidence over dynamic trajectories from different modalities (e.g., intrinsic or extrinsic) and hierarchical locations (e.g., elbow or end effector), ultimately solving the task via inference.

2.2.1 Model analysis

Figure 5 shows a sequence of time frames for the task described. Although both objects are moving, the discrete model can infer and impose continuous trajectories that allow it to operate in a dynamic environment. The beliefs over the hidden states are initialized at the real starting configuration of the arm. At the beginning of the trial, the agent infers two possible kinematic configurations for the tool and the ball. While the two observations of the tool constrain the corresponding inference, the ball belief is only subject to its actual position, thus letting the agent initially overestimate

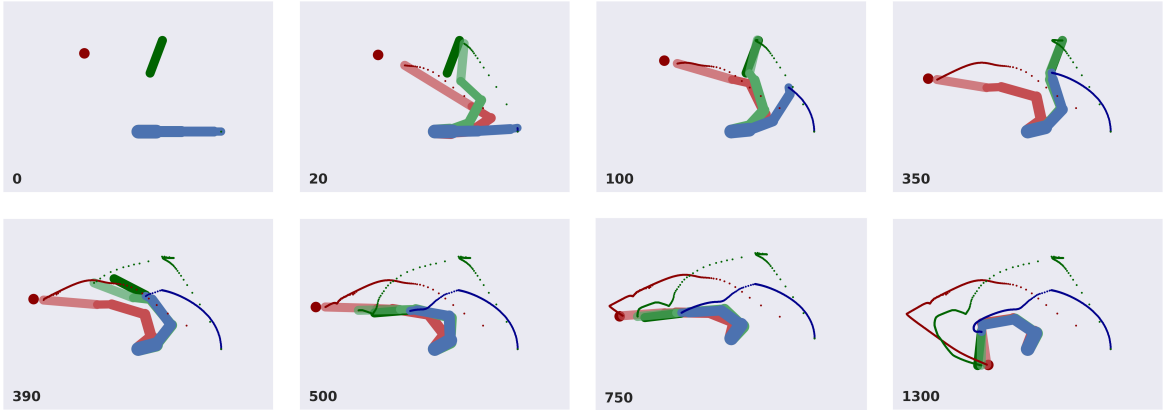


Figure 5: Sequence of time frames of the simulation. Real ball, tool, and end effector are displayed in dark red, dark green, and dark blue respectively. Beliefs over every environmental entity, in terms of kinematic configurations, are shown in light red, light green, and light blue. Trajectories of the end effector, tool, and ball are displayed as well. The number of time steps is shown in the lower-left corner of each frame.

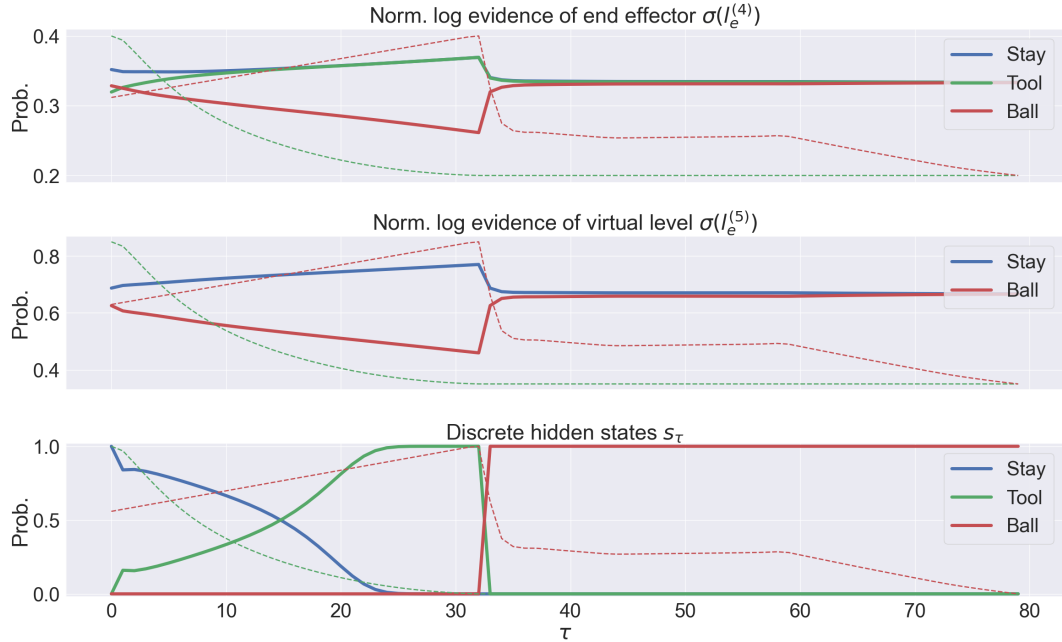


Figure 6: Normalized log evidences, for each discrete step τ (composed, in turn, of 10 continuous time steps), of the end effector level $l_e^{(4)}$ (top), and virtual level $l_e^{(5)}$ (middle). Discrete hidden states (bottom). The green and red dashed lines respectively represent the tool’s extremity-ball distance, and the tool’s origin-end effector distance, normalized to fit in the plots. As explained in Appendix D, the agent has two hidden causes related to the steps of the task, i.e., reaching the ball and reaching the tool, and an additional *stay* cause.

the length of the virtual level. During the first phase, only the tool reaching intention is active: as a consequence, the tool belief constantly biases the arm belief, which in turn pulls the real arm. After 350 steps, both these beliefs are in the same configuration, while the ball belief has inferred the corresponding position. At this point, the tool is grasped, causing the discrete model to predict a different combination of hidden causes. Now, both the tool and arm beliefs are pulled toward the ball belief. After about 800 steps, the agent infers the same configuration for all three beliefs, managing to reach the ball with the tool’s extremity, and tracking it until the end of the trial. Note how even during the first reaching movement, the agent constantly updates its configuration in relation to the ball; as a result, the second reaching movement will be faster.

The transitions can be better appreciated from Figure 6, showing the bottom-up messages of the accumulated evidences $l_e^{(4)}$ and $l_e^{(5)}$ for the last two levels of the hierarchy (i.e., end effector and tool), and the discrete hidden states s_τ . As evident, the virtual level does not contribute to the inference of the first intention, since this only involves the end effector. Note how the agent is able to dynamically accumulate the evidences over its hypotheses: during the first phase, the evidence $l_{e,t}^{(4)}$ increases as soon as the end effector approaches the tool’s origin, while $l_{e,b}^{(4)}$ and $l_{e,b}^{(5)}$ decrease as the ball moves away. During the second phase, the latter two rapidly increase as the end effector approaches the ball; finally, every hidden cause of both levels slowly stabilizes as the extrinsic beliefs converge to the same value and the errors are minimized. The slow decrease of the initial state and the fast transition between the two steps are well summarized in the bottom graph. The trajectories of the hidden states show that the agent can plan new intentions with a high frequency (in this case, 10 continuous time steps), allowing it to react rapidly to environmental stimuli.

In order to assess the model performances in dynamic planning tasks, we run 100 simulations by randomly sampling the ball position and direction, and 100 simulations by randomly sampling both ball and tool positions and directions. The width and height of the virtual environment were 3 times the total arm length, hence the ball and tool were out of reach for a significant period of each trial. The duration of each trial was set to 3000 steps. In the first case, the agent managed to reach the ball with the tool in 91% of trials, with a mean reaction time of 1098 steps and std. of 656. In the second case, the accuracy decreased to 53% given the higher difficulty of the task, with a mean reaction time of 1588 steps and std. of 719.

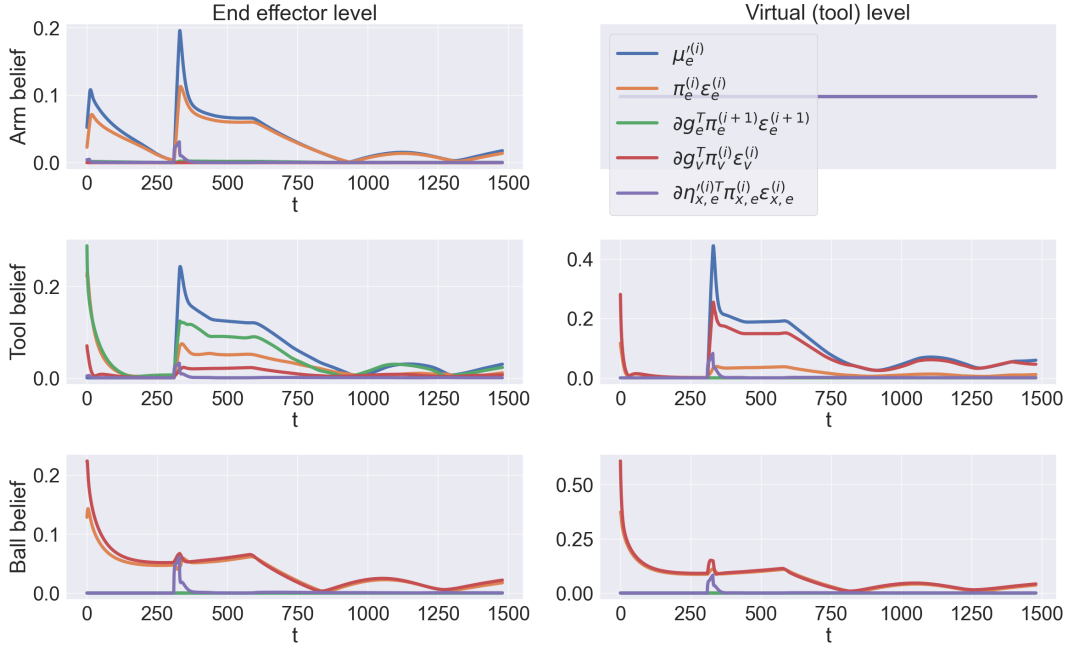


Figure 7: Trajectory of every component of the extrinsic belief updates for the end effector (left panels), and virtual (right panels) levels. Every environmental entity is shown separately. Blue, orange, green, red, and purple lines respectively indicate the 1st-order derivative, the extrinsic prediction error from the previous level, the extrinsic prediction error from the next level, the visual prediction error, and the backward dynamics error.

The dynamic behavior of the extrinsic beliefs can be analyzed from Figure 7, showing the trajectories of all the forces that make up the update of Equation 55, for the last two levels and every environmental entity. The transition between the two phases of the task is here evident: the 1st-order derivative of the arm belief $\mu_{e,a}^{(4)}$ (blue line in the top left panel) is non-zero during the whole task, and presents two spikes at the beginning of each phase, signaling an increased prediction error due to the new intention. The arm movement during the first phase is the consequence of the non-zero 1st-order derivative of the tool belief $\mu_{e,t}^{(4)}$ (blue line in the middle left panel).

The dynamics of the corresponding extrinsic prediction error $\varepsilon_{e,t}^{(5)}$ (green line in the middle left panel) combines both this derivative and the visual prediction error of the next level $\varepsilon_{v,t}^{(5)}$ (red line in the middle right panel). Note that this

extrinsic prediction error does not exist for the arm belief, and that the backward dynamics error $\varepsilon_{e,x,a}^{(4)}$ has a smaller impact on the overall update with respect to the 1st-order derivative. The second phase begins with a spike in the 1st-order derivative of the tool belief at the virtual level $\mu_{e,t}^{(5)}$ (blue line in the middle right panel), which is propagated back to the previous level as an extrinsic prediction error. Finally, note that the ball belief is only subject to its visual observation and the extrinsic prediction error coming from the previous levels.

3 Discussion

In this study, we developed a computational method that affords dynamic planning in active inference. The goal was twofold. First, to show the effectiveness of casting control problems as inference and, in particular, of expressing entities in relation to a hierarchical configuration of the self. While there could be several ways to combine the units of the proposed architecture, we showed a specific design as a proof-of-concept to solve a non-trivial task: reaching a moving object with a tool. The agent had to rely on three kinds of depth, i.e., it had to dynamically infer its intentions for decision-making, and form different hierarchical generative models depending on the structure and affordances of the entities.

Most importantly, our goal was to show that a (deep) hierarchical formulation of active inference lends itself to learning and generalization of novel tasks. Although we used a fixed generative model, we revealed that an advanced behavior is possible by using simple likelihood and dynamics functions, and by decomposing the model into small units linked together. In [61], a hierarchical kinematic model was used to learn the segments of an agent’s kinematic chain, both during perception and action. Therefore, an encouraging research direction would be to design a hierarchical hybrid model in the wake of PCNs or traditional neural networks, and let the agent learn appropriate structure and internal attractors for a specific goal via free energy minimization. A common criticism of deep RL is that it lacks explainability, which is of greater concern as AI systems rapidly grow. A viable alternative is to learn a model of the environment [62], e.g., with Bayesian non-parametrics [63]; however, these approaches are still computationally demanding. Albaracín and colleagues described how active inference may find an answer to the *black box problem* [64], and we further showed how different elements of an active inference agent have practical and interpretable meanings. In this view, optimization of parameters in hybrid models could be an effective alternative to deep RL algorithms, or other approaches in active inference relying on the use of neural networks as generative models.

Another important limitation of the proposed model is that it relied on just two temporal orders, and a more complete and effective model would make use of generalized coordinates [65]. Indeed, every aspect that we introduced can be extended by considering increasing temporal orders. For instance, discrete variables could depend on the position, velocity, and acceleration of an object, thus inferring a more accurate representation of dynamic trajectories. Also, flexible behavior could be specified in the 2nd temporal order, resulting in a more realistic force-controlled system.

An interesting direction of research regards the generation of states and paths. Some implementations of discrete models used additional connections between policies and between discrete hidden states [66, 49]; hence, it might be worth designing such kinds of links in continuous and hybrid contexts as well. In this study, a single high-level discrete model imposed the behavior of every other hybrid unit; an alternative would be to design independent connections between hidden causes, such that a high-level intention would be propagated down to lower levels with local message passing. This approach may also provide insights into how, by repetition of the same task, discrete policies adapt to construct composite movements (e.g., a reaching and grasping action) from simpler continuous intentions.

Finally, hybrid units can impose and infer dynamic trajectories for the whole period of continuous evidence accumulation, but cannot perform decision-making alone. Another approach would be to consider a complete discrete-continuous model (i.e., Figure 2) as the most basic unit, permitting local decision-making and affording a much richer behavior at intermediate levels. Alternatively, a hierarchical discrete model – and not just a single level – can be implemented on top of the hybrid architecture, with the possibility for supervised structure learning and planning at various discrete timescales [67].

Acknowledgments

This research received funding from the European Union’s Horizon H2020-EIC-FETPROACT-2019 Programme for Research and Innovation under Grant Agreement 951910 to I.P.S. The funders had no role in study design, data collection and analysis, decision to publish, or preparation of the manuscript.

References

- [1] R.S. Sutton and A.G. Barto. Reinforcement learning: An introduction. *IEEE Transactions on Neural Networks*, 9(5):1054–1054, 1998.
- [2] Aravind Rajeswaran, Vikash Kumar, Abhishek Gupta, Giulia Vezzani, John Schulman, Emanuel Todorov, and Sergey Levine. Learning complex dexterous manipulation with deep reinforcement learning and demonstrations. In *Proceedings of Robotics: Science and Systems*, Pittsburgh, Pennsylvania, June 2018.
- [3] Beren Millidge, Tommaso Salvatori, Yuhang Song, Rafal Bogacz, and Thomas Lukasiewicz. Predictive Coding: Towards a Future of Deep Learning beyond Backpropagation? *IJCAI International Joint Conference on Artificial Intelligence*, pages 5538–5545, 2022.
- [4] Jakob Hohwy. *The Predictive Mind*. Oxford University Press UK, 2013.
- [5] Rajesh P.N. Rao and Dana H. Ballard. Predictive coding in the visual cortex: A functional interpretation of some extra-classical receptive-field effects. *Nature Neuroscience*, 2(1):79–87, 1999.
- [6] Andy Clark. Whatever next? Predictive brains, situated agents, and the future of cognitive science. *Behavioral and Brain Sciences*, 36(3):181–204, 2013.
- [7] H. Kobayashi and L. R. Bahl. Image data compression by predictive coding i: Prediction algorithms. *IBM Journal of Research and Development*, 18(2):164–171, 1974.
- [8] Alexander Ororbia and Daniel Kifer. The neural coding framework for learning generative models. *Nature Communications*, 13(1), 2022.
- [9] Tommaso Salvatori, Ankur Mali, Christopher L. Buckley, Thomas Lukasiewicz, Rajesh P. N. Rao, Karl Friston, and Alexander Ororbia. Brain-inspired computational intelligence via predictive coding, 2023.
- [10] James C R Whittington and Rafal Bogacz. An approximation of the error backpropagation algorithm in a predictive coding network with local hebbian synaptic plasticity. *Neural Comput*, 29(5):1229–1262, March 2017.
- [11] James C.R. Whittington and Rafal Bogacz. Theories of Error Back-Propagation in the Brain. *Trends in Cognitive Sciences*, 23(3):235–250, 2019.
- [12] Beren Millidge, Alexander Tschantz, and Christopher L. Buckley. Predictive Coding Approximates Backprop Along Arbitrary Computation Graphs. *Neural Computation*, 34(6):1329–1368, 2022.
- [13] Tommaso Salvatori, Yuhang Song, Thomas Lukasiewicz, Rafal Bogacz, and Zhenghua Xu. Predictive coding can do exact backpropagation on convolutional and recurrent neural networks, 2021.
- [14] Beren Millidge. Combining Active Inference and Hierarchical Predictive Coding: a Tutorial Introduction and Case Study. *PsyArXiv*, 2019.
- [15] Ivilin Stoianov, Domenico Maisto, and Giovanni Pezzulo. The hippocampal formation as a hierarchical generative model supporting generative replay and continual learning. *Progress in Neurobiology*, 217(102329):1–20, 2022.
- [16] Alexander Ororbia and Ankur Mali. Active Predicting Coding: Brain-Inspired Reinforcement Learning for Sparse Reward Robotic Control Problems. 2022.
- [17] Rajesh P. N. Rao, Dimitrios C. Gklezakos, and Vishwas Sathish. Active predictive coding: A unified neural framework for learning hierarchical world models for perception and planning, 2022.
- [18] Beren Millidge, Mahyar Osanlouy, and Rafal Bogacz. Predictive Coding Networks for Temporal Prediction. pages 1–59, 2023.
- [19] Ares Fisher and Rajesh P N Rao. Recursive neural programs: A differentiable framework for learning compositional part-whole hierarchies and image grammars. *PNAS Nexus*, 2(11), October 2023.

[20] Karl J. Friston, Tamara Shiner, Thomas FitzGerald, Joseph M. Galea, Rick Adams, Harriet Brown, Raymond J. Dolan, Rosalyn Moran, Klaas Enno Stephan, and Sven Bestmann. Dopamine, affordance and active inference. *PLoS Computational Biology*, 8(1):e1002327, January 2012.

[21] Larry S Zweifel, Jonathan P Fadok, Emmanuel Argilli, Michael G Garelick, Graham L Jones, Tavis M K Dickerson, James M Allen, Sheri J Y Mizumori, Antonello Bonci, and Richard D Palmiter. Activation of dopamine neurons is critical for aversive conditioning and prevention of generalized anxiety. *Nature Neuroscience*, 14(5):620–626, 2011.

[22] Karl J. Friston, Jean Daunizeau, and Stefan J. Kiebel. Reinforcement learning or active inference? *PLoS ONE*, 4(7), 2009.

[23] Karl Friston. What is optimal about motor control? *Neuron*, 72(3):488–498, 2011.

[24] Karl J. Friston, Jean Daunizeau, James Kilner, and Stefan J. Kiebel. Action and behavior: A free-energy formulation. *Biological Cybernetics*, 102(3):227–260, 2010.

[25] Karl Friston. The free-energy principle: A unified brain theory? *Nature Reviews Neuroscience*, 11(2):127–138, 2010.

[26] Thomas Parr, Giovanni Pezzulo, and Karl J Friston. *Active inference: the free energy principle in mind, brain, and behavior*. Cambridge, MA: MIT Press, 2021.

[27] Matteo Priorelli, Federico Maggiore, Antonella Maselli, Francesco Donnarumma, Domenico Maisto, Francesco Mannella, Ivilin Peev Stoianov, and Giovanni Pezzulo. Modeling motor control in continuous-time Active Inference: a survey. *IEEE Transactions on Cognitive and Developmental Systems*, pages 1–15, 2023.

[28] Thomas Parr and Karl J. Friston. Uncertainty, epistemics and active inference. *Journal of The Royal Society Interface*, 14(136):20170376, November 2017.

[29] Beren Millidge, Alexander Tschantz, Anil K. Seth, and Christopher L. Buckley. On the relationship between active inference and control as inference. *Communications in Computer and Information Science*, 1326:3–11, 2020.

[30] Matthew Botvinick and Marc Toussaint. Planning as inference. *Trends in Cognitive Sciences*, 16(10):485–488, 2012.

[31] Marc Toussaint and Amos Storkey. Probabilistic inference for solving discrete and continuous state Markov Decision Processes. *ACM International Conference Proceeding Series*, 148:945–952, 2006.

[32] Marc Toussaint. Probabilistic inference as a model of planned behavior. *Künstliche Intelligenz*, 3/09:23–29, 2009.

[33] Karl Friston. Hierarchical models in the brain. *PLoS Computational Biology*, 4(11), 2008.

[34] Karl J. Friston, Thomas Parr, Yan Yufik, Noor Sajid, Catherine J. Price, and Emma Holmes. Generative models, linguistic communication and active inference. *Neuroscience & Biobehavioral Reviews*, 118:42–64, November 2020.

[35] Kai Ueltzhöffer. Deep Active Inference. pages 1–40, 2017.

[36] Beren Millidge. Deep active inference as variational policy gradients. *Journal of Mathematical Psychology*, 96, 2020.

[37] Zafeirios Fountas, Noor Sajid, Pedro A.M. Mediano, and Karl Friston. Deep active inference agents using Monte-Carlo methods. *Advances in Neural Information Processing Systems*, 2020-Decem(NeurIPS), 2020.

[38] Thomas Rood, Marcel van Gerven, and Pablo Lanillos. A deep active inference model of the rubber-hand illusion. 2020.

[39] Cansu Sancaktar, Marcel A. J. van Gerven, and Pablo Lanillos. End-to-End Pixel-Based Deep Active Inference for Body Perception and Action. In *2020 Joint IEEE 10th International Conference on Development and Learning and Epigenetic Robotics (ICDL-EpiRob)*, pages 1–8, 2020.

[40] Théophile Champion, Marek Grześ, Lisa Bonheme, and Howard Bowman. Deconstructing deep active inference. 2023.

[41] Aleksey Zelenov and Vladimir Krylov. Deep active inference in control tasks. In *2021 International Conference on Electrical, Communication, and Computer Engineering (ICECCE)*, pages 1–3, 2021.

[42] Ozan Çatal, Tim Verbelen, Toon Van de Maele, Bart Dhoedt, and Adam Safron. Robot navigation as hierarchical active inference. *Neural Networks*, 142:192–204, 2021.

[43] Kai Yuan, Karl Friston, Zhibin Li, and Noor Sajid. Hierarchical generative modelling for autonomous robots. *Research Square*, 2023.

[44] Matteo Priorelli, Giovanni Pezzulo, and Ivilin Peev Stoianov. Deep kinematic inference affords efficient and scalable control of bodily movements. *PNAS*, 120, 2023.

[45] Karl J. Friston, Thomas Parr, and Bert de Vries. The graphical brain: Belief propagation and active inference. 1(4):381–414, 2017.

[46] Karl J. Friston, Richard Rosch, Thomas Parr, Cathy Price, and Howard Bowman. Deep temporal models and active inference. *Neuroscience and Biobehavioral Reviews*, 77(November 2016):388–402, 2017.

[47] Thomas Parr and Karl J. Friston. Active inference and the anatomy of oculomotion. *Neuropsychologia*, 111(January):334–343, 2018.

[48] T. Parr and K. J. Friston. The computational pharmacology of oculomotion. *Psychopharmacology (Berl.)*, 236(8):2473–2484, August 2019.

[49] Karl J. Friston, Thomas Parr, Conor Heins, Axel Constant, Daniel Friedman, Takuya Isomura, Chris Fields, Tim Verbelen, Maxwell Ramstead, John Clippinger, and Christopher D. Frith. Federated inference and belief sharing. *Neuroscience & Biobehavioral Reviews*, 156:105500, 2024.

[50] Karl Friston and Will Penny. Post hoc Bayesian model selection. *NeuroImage*, 56(4):2089–2099, 2011.

[51] Karl Friston, Thomas Parr, and Peter Zeidman. Bayesian model reduction. pages 1–32, 2018.

[52] Thomas Parr and Karl J. Friston. The Discrete and Continuous Brain: From Decisions to Movement—And Back Again Thomas. *Neural Computation*, 30:2319–2347, 2018.

[53] M. Priorelli and I.P. Stoianov. Dynamic inference by model reduction. *bioRxiv*, 2023.

[54] Rick A. Adams, Stewart Shipp, and Karl J. Friston. Predictions not commands: Active inference in the motor system. *Brain Structure and Function*, 218(3):611–643, 2013.

[55] Léo Pio-Lopez, Ange Nizard, Karl Friston, and Giovanni Pezzulo. Active inference and robot control: A case study. *Journal of the Royal Society Interface*, 13(122), 2016.

[56] Matteo Priorelli and Ivilin Peev Stoianov. Slow but flexible or fast but rigid? discrete and continuous processes compared. *bioRxiv*, 2023.

[57] Rick A. Adams, Eduardo Aponte, Louise Marshall, and Karl J. Friston. Active inference and oculomotor pursuit: The dynamic causal modelling of eye movements. *Journal of Neuroscience Methods*, 242:1–14, 2015.

[58] Matteo Priorelli and Ivilin Peev Stoianov. Dynamic planning in hierarchical active inference. *arXiv*, 2024.

[59] Karl Friston, Lancelot Da Costa, Danijar Hafner, Casper Hesp, and Thomas Parr. Sophisticated inference. *Neural Computation*, 33(3):713–763, 2021.

[60] M. Priorelli, G. Pezzulo, and I.P. Stoianov. Active vision in binocular depth estimation: A top-down perspective. *Biomimetics*, 8(5), 2023.

[61] Matteo Priorelli and Ivilin Peev Stoianov. Efficient motor learning through action-perception cycles in deep kinematic inference. In *Active Inference*, pages 59–70. Springer Nature Switzerland, 2024.

[62] Thomas M. Moerland, Joost Broekens, Aske Plaat, and Catholijn M. Jonker. Model-based reinforcement learning: A survey. 2022.

[63] I Stoianov, C Pennartz, C Lansink, and G Pezzulo. Model-based spatial navigation in the hippocampus-ventral striatum circuit: a computational analysis. *Plos Computational Biology*, 14(9):1–28, 2018.

[64] Mahault Albarracin, Inês Hipólito, Safaei Essafi Tremblay, Jason G. Fox, Gabriel René, Karl Friston, and Maxwell J. D. Ramstead. Designing explainable artificial intelligence with active inference: A framework for transparent introspection and decision-making. 2023.

[65] Karl Friston, Klaas Stephan, Baojuan Li, and Jean Daunizeau. Generalised filtering. *Mathematical Problems in Engineering*, 2010:Article ID 621670, 34 p.–Article ID 621670, 34 p., 2010.

- [66] Toon Van de Maele, Tim Verbelen, Pietro Mazzaglia, Stefano Ferraro, and Bart Dhoedt. Object-centric scene representations using active inference, 2023.
- [67] Karl J. Friston, Lancelot Da Costa, Alexander Tschantz, Alex Kiefer, Tommaso Salvatori, Victorita Neacsu, Magnus Koudahl, Conor Heins, Noor Sajid, Dimitrije Markovic, Thomas Parr, Tim Verbelen, and Christopher L Buckley. Supervised structure learning. 2023.
- [68] Jakob Hohwy. New directions in predictive processing. *Mind and Language*, 35(2):209–223, 2020.
- [69] Karl Friston and Stefan Kiebel. Predictive coding under the free-energy principle. *Philosophical Transactions of the Royal Society B: Biological Sciences*, 364(1521):1211–1221, 2009.
- [70] Michael I. Jordan, Zoubin Ghahramani, Tommi S. Jaakkola, and Lawrence K. Saul. *Machine Learning*, 37(2):183–233, 1999.
- [71] Thomas Parr, Giovanni Pezzulo, and Karl J Friston. Active inference: the free energy principle in mind, brain, and behavior. 2022.
- [72] Karl Friston, Lancelot Da Costa, Noor Sajid, Conor Heins, Kai Ueltzhöffer, Grigoris A. Pavliotis, and Thomas Parr. The free energy principle made simpler but not too simple. *Physics Reports*, 1024:1–29, 2022.
- [73] Giovanni Pezzulo, Francesco Rigoli, and Karl J. Friston. Hierarchical Active Inference: A Theory of Motivated Control. *Trends in Cognitive Sciences*, 22(4):294–306, 2018.
- [74] Karl J. Friston and Christopher D. Frith. Active inference, communication and hermeneutics. *Cortex*, 68:129–143, July 2015.
- [75] Thomas Parr and Karl J. Friston. Generalised free energy and active inference. *Biological Cybernetics*, 113(5–6):495–513, September 2019.
- [76] Ryan Smith, Karl J. Friston, and Christopher J. Whyte. A step-by-step tutorial on active inference and its application to empirical data. *Journal of Mathematical Psychology*, 107:102632, 2022.
- [77] Lancelot Da Costa, Thomas Parr, Noor Sajid, Sebastijan Veselic, Victorita Neacsu, and Karl Friston. Active inference on discrete state-spaces: A synthesis. *Journal of Mathematical Psychology*, 99, 2020.
- [78] Karl Friston, Jérémie Mattout, Nelson Trujillo-Barreto, John Ashburner, and Will Penny. Variational free energy and the Laplace approximation. *NeuroImage*, 34(1):220–234, 2007.
- [79] Matteo Priorelli and Ivilin Peev Stoianov. Flexible Intentions: An Active Inference Theory. *Frontiers in Computational Neuroscience*, 17:1 – 41, 2023.

A Predictive coding networks

The theory of predictive coding (PC) builds on the premise that the human brain makes sense of the world by constructing a generative model of how hidden states of the real environment generate the perceived sensations [5, 6, 68]. This internal model is continuously refined by minimizing the discrepancy (called *prediction error*) between sensory predictions and the sensations. More formally, given some prior knowledge $p(\mathbf{x})$ over hidden states \mathbf{x} and partial evidence $p(\mathbf{y})$ over sensation \mathbf{y} , the nervous system can find the posterior distribution of the hidden states given the sensations via Bayes rule:

$$p(\mathbf{x}|\mathbf{y}) = \frac{p(\mathbf{x}, \mathbf{y})}{p(\mathbf{x})} \quad (14)$$

However, direct computation of the posterior $p(\mathbf{x}|\mathbf{y})$ is unfeasible since the evidence requires marginalizing over every possible outcome, i.e., $p(\mathbf{y}) = \int p(\mathbf{x}, \mathbf{y}) d\mathbf{x}$. Hence, predictive coding supposes that instead of performing exact Bayesian inference, organisms are engaged in a variational approach [69], i.e., they approximate the posterior distribution with a simpler *recognition* distribution $q(\mathbf{x}) \approx p(\mathbf{x}|\mathbf{y})$, and minimize the difference between the two distributions. This difference is expressed in terms of a Kullback-Leibler (KL) divergence:

$$D_{KL}[q(\mathbf{x})||p(\mathbf{x}|\mathbf{y})] = \int_{\mathbf{x}} q(\mathbf{x}) \ln \frac{q(\mathbf{x})}{p(\mathbf{x}|\mathbf{y})} d\mathbf{x} \quad (15)$$

Given that the denominator $p(\mathbf{x}|\mathbf{y})$ still depends on the marginal $p(\mathbf{y})$, we express the KL divergence in terms of the log evidence and the *Variational Free Energy* (VFE), and minimize the latter quantity instead. The VFE is the negative of what in the machine learning community is known as the *evidence lower bound* or *ELBO* [70]:

$$\mathcal{F} = \mathbb{E}_{q(\mathbf{x})} \left[\ln \frac{q(\mathbf{x})}{p(\mathbf{x}, \mathbf{y})} \right] = \mathbb{E}_{q(\mathbf{x})} \left[\ln \frac{q(\mathbf{x})}{p(\mathbf{x}|\mathbf{y})} \right] - \ln p(\mathbf{y}) \quad (16)$$

Since the KL divergence is always nonnegative, the VFE provides an upper bound on surprise, i.e., $\mathcal{F} \geq \ln p(\mathbf{y})$. Therefore, minimizing the KL divergence with respect to $q(\mathbf{x})$ is equivalent to minimizing \mathcal{F} . The more the VFE approaches 0, the closer the approximate distribution is to the real posterior, and the higher will be the model evidence (or, equivalently, the lower will be the surprise about sensory outcomes). The discrepancy between the two distributions also depends on the specific assumptions made over the recognition distribution: a common one is the Laplace approximation [69], which assumes Gaussian probability distributions, e.g., $q(\mathbf{x}) = \mathcal{N}(\boldsymbol{\mu}, \boldsymbol{\Sigma})$, where $\boldsymbol{\mu}$ represents the most plausible hypothesis - also called *belief* about the hidden states \mathbf{x} - and $\boldsymbol{\Sigma}$ is its covariance matrix. Now, we factorize the generative model $p(\mathbf{x}, \mathbf{y})$ into likelihood and prior terms, and we further parameterize it with some parameters $\boldsymbol{\theta}$:

$$\begin{aligned} p(\mathbf{x}, \mathbf{y}) &= p(\mathbf{x}|\mathbf{y}, \boldsymbol{\theta})p(\mathbf{x}) \\ p(\mathbf{y}|\mathbf{x}, \boldsymbol{\theta}) &= \mathcal{N}(\mathbf{g}(\mathbf{x}, \boldsymbol{\theta}), \boldsymbol{\Sigma}_y) \\ p(\mathbf{x}) &= \mathcal{N}(\boldsymbol{\eta}, \boldsymbol{\Sigma}_\eta) \end{aligned} \quad (17)$$

where $\mathbf{g}(\mathbf{x}, \boldsymbol{\theta})$ is a likelihood function and $\boldsymbol{\eta}$ is a prior. In this way, the VFE breaks down to the following simple formula:

$$\mathcal{F} = -\frac{1}{2} [\boldsymbol{\Pi}_y \boldsymbol{\varepsilon}_y^2 + \boldsymbol{\Pi}_\eta \boldsymbol{\varepsilon}_\eta^2 + \ln 2\pi \boldsymbol{\Sigma}_y + \ln 2\pi \boldsymbol{\Sigma}_\eta] \quad (18)$$

where we expressed the difference in the exponents of the Gaussian distributions in terms of *prediction errors* $\boldsymbol{\varepsilon}_y = \mathbf{y} - \mathbf{g}(\mathbf{x}, \boldsymbol{\theta})$ and $\boldsymbol{\varepsilon}_\eta = \boldsymbol{\mu} - \boldsymbol{\eta}$, and we wrote the covariances in terms of their inverse, i.e., precisions $\boldsymbol{\Pi}_y$ and $\boldsymbol{\Pi}$. In order to minimize the KL divergence between the real and approximate posteriors, we can minimize the VFE with respect to the beliefs $\boldsymbol{\mu}$ - a process associated with *perception* - and the parameters $\boldsymbol{\theta}$ - generally referred to as *learning*. In practice, the update rules follow gradient descent:

$$\begin{aligned} \boldsymbol{\mu} &= \arg \min_{\boldsymbol{\mu}} \mathcal{F} & \boldsymbol{\theta} &= \arg \min_{\boldsymbol{\theta}} \mathcal{F} \\ \dot{\boldsymbol{\mu}} &= -\partial_{\boldsymbol{\mu}} \mathcal{F} = \partial_{\boldsymbol{\mu}} \mathbf{g}^T \boldsymbol{\Pi}_y \boldsymbol{\varepsilon}_y - \boldsymbol{\Pi}_\eta \boldsymbol{\varepsilon}_\eta & \dot{\boldsymbol{\theta}} &= -\partial_{\boldsymbol{\theta}} \mathcal{F} = -\partial_{\boldsymbol{\theta}} \mathbf{g}^T \boldsymbol{\Pi}_y \boldsymbol{\varepsilon}_y \end{aligned} \quad (19)$$

In order to separate the timescales of fast perception and slow-varying learning, the two phases are treated as the steps of an EM algorithm, i.e., optimizing the beliefs while keeping fixed the parameters, and then optimizing the parameters while keeping fixed the beliefs.

This simple predictive coding algorithm can be scaled up to learn highly complex structures, called *Predictive Coding Networks* (PCNs) [3, 9], composed of causal relationships of arbitrarily high depth – in a similar way to deep neural networks. In particular, we can factorize a generative model into a product of different distributions, wherein a specific level only depends on the level above:

$$\begin{aligned} p(\mathbf{x}^{(0)}, \dots, \mathbf{x}^{(l)}) &= p(\mathbf{x}^{(0)}) \prod_{l=1}^L p(\mathbf{x}^{(l)} | \mathbf{x}^{(l-1)}) \\ p(\mathbf{x}^{(l)} | \mathbf{x}^{(l-1)}) &= \mathcal{N}(\mathbf{g}(\mathbf{x}^{(l-1)}, \boldsymbol{\theta}^{(l-1)}), \boldsymbol{\Sigma}^{(l)}) \end{aligned} \quad (20)$$

where 0 indicates the highest level, and L is the number of levels in the hierarchy. In this way, $\mathbf{x}^{(l)}$ acts as an observation for level $l - 1$, and $\mathbf{g}(\mathbf{x}^{(l)}, \boldsymbol{\theta}^{(l)})$ acts as a prior for level $l + 1$. As a result, this factorization allows us to express the update of beliefs and parameters of a specific level only based on the level above and the level below – hence treating the VFE minimization as in the simple case described before. Differently from the backpropagation algorithm of neural networks, the message passing of prediction errors implements a biologically plausible Hebbian rule between presynaptic and postsynaptic activities. In fact, the predictions \mathbf{u} computed by the likelihood functions are typically a weighted combination of neurons passed to a nonlinear activation function ϕ :

$$\mathbf{u}_i^{(l)} = \sum_{j=1}^J \mathbf{W}_{i,j}^{(l-1)} \phi(\mathbf{x}_j^{(l-1)}) \quad (21)$$

where $W_{i,j}^{(l-1)}$ are the weights from neuron j at level $l - 1$ to neuron i at level l . Crucially, what is backpropagated in PCNs are not signals detecting increasingly complex features, but messages representing how much the model is *surprised* about sensory observations (e.g., a prediction equal to an observation means that the network structure is a good approximation of the real process, and no errors have to be conveyed).

B Hierarchical active inference

The theory of active inference starts with the same assumptions of predictive coding, but with two critical differences. The first one – which is actually shared with some implementations of predictive coding such as temporal PC – assumes that living organisms constantly deal with highly dynamic environments, and the internal models that they build must reflect the changes occurring in the real generative process [52]. This relation is usually expressed in terms of generalized coordinates of motion (encoding, e.g., position, velocity, acceleration, and so on) [65]; consequently, the environment is modeled with the following nonlinear system:

$$\begin{aligned} \tilde{\mathbf{y}} &= \tilde{\mathbf{g}}(\tilde{\mathbf{x}}) + \mathbf{w}_y \\ \mathcal{D}\tilde{\mathbf{x}} &= \tilde{\mathbf{f}}(\tilde{\mathbf{x}}, \tilde{\mathbf{v}}) + \mathbf{w}_x \end{aligned} \quad (22)$$

where $\tilde{\mathbf{x}}$ are the generalized hidden states, $\tilde{\mathbf{v}}$ are the generalized hidden causes (whose role will be clear soon), $\tilde{\mathbf{y}}$ are the generalized sensory signals, \mathcal{D} is a differential operator that shifts all the temporal orders by one, i.e.: $\mathcal{D}\tilde{\mathbf{x}} = [\mathbf{x}', \mathbf{x}'', \mathbf{x}''', \dots]$, and the letter w indicates noise terms assumed to be sampled from a Gaussian distribution. The likelihood function $\tilde{\mathbf{g}}$ defines how hidden states generate (generalized) sensory observations (as in predictive coding), while the dynamics function $\tilde{\mathbf{f}}$ specify the evolution of the temporal orders of the hidden states (see [71, 72] for more details). The associated joint probability is factorized into independent distributions:

$$p(\tilde{\mathbf{y}}, \tilde{\mathbf{x}}, \tilde{\mathbf{v}}) = p(\tilde{\mathbf{y}} | \tilde{\mathbf{x}})p(\tilde{\mathbf{x}} | \tilde{\mathbf{v}})p(\tilde{\mathbf{v}}) \quad (23)$$

where each distribution is Gaussian:

$$\begin{aligned} p(\tilde{\mathbf{y}}|\tilde{\mathbf{x}}) &= \mathcal{N}(\tilde{\mathbf{g}}(\tilde{\mathbf{x}}), \tilde{\mathbf{\Pi}}_y^{-1}) \\ p(\mathcal{D}\tilde{\mathbf{x}}|\tilde{\mathbf{v}}) &= \mathcal{N}(\tilde{\mathbf{f}}(\tilde{\mathbf{x}}, \tilde{\mathbf{v}}), \tilde{\mathbf{\Pi}}_x^{-1}) \\ p(\tilde{\mathbf{v}}|\boldsymbol{\eta}) &= \mathcal{N}(\boldsymbol{\eta}, \tilde{\mathbf{\Pi}}_v^{-1}) \end{aligned} \quad (24)$$

expressed in terms of precisions $\tilde{\mathbf{\Pi}}_y$, $\tilde{\mathbf{\Pi}}_x$, and $\tilde{\mathbf{\Pi}}_v$. As in predictive coding, these distributions are inferred through approximate posteriors $q(\tilde{\mathbf{x}})$ and $q(\tilde{\mathbf{v}})$, minimizing the related VFE \mathcal{F} . As a result, the updates of the beliefs $\tilde{\boldsymbol{\mu}}$ and $\tilde{\boldsymbol{\nu}}$ respectively over the hidden states and hidden causes become:

$$\begin{aligned} \dot{\tilde{\boldsymbol{\mu}}} - \mathcal{D}\tilde{\boldsymbol{\mu}} &= -\partial_\mu \mathcal{F} = \partial \tilde{\mathbf{g}}^T \tilde{\mathbf{\Pi}}_y \tilde{\boldsymbol{\varepsilon}}_y + \partial_\mu \tilde{\mathbf{f}}^T \tilde{\mathbf{\Pi}}_x \tilde{\boldsymbol{\varepsilon}}_x - \mathcal{D}^T \tilde{\mathbf{\Pi}}_x \tilde{\boldsymbol{\varepsilon}}_x \\ \dot{\tilde{\boldsymbol{\nu}}} - \mathcal{D}\tilde{\boldsymbol{\nu}} &= -\partial_\nu \mathcal{F} = \partial_\nu \tilde{\mathbf{f}}^T \tilde{\mathbf{\Pi}}_x \tilde{\boldsymbol{\varepsilon}}_x - \tilde{\mathbf{\Pi}}_v \tilde{\boldsymbol{\varepsilon}}_v \end{aligned} \quad (25)$$

where $\tilde{\boldsymbol{\varepsilon}}_y$, $\tilde{\boldsymbol{\varepsilon}}_x$, and $\tilde{\boldsymbol{\varepsilon}}_v$ are respectively the prediction errors of sensory signals, dynamics, and priors:

$$\begin{aligned} \tilde{\boldsymbol{\varepsilon}}_y &= \tilde{\mathbf{y}} - \tilde{\mathbf{g}}(\tilde{\boldsymbol{\mu}}) \\ \tilde{\boldsymbol{\varepsilon}}_x &= \mathcal{D}\tilde{\boldsymbol{\mu}} - \tilde{\mathbf{f}}(\tilde{\boldsymbol{\mu}}, \tilde{\boldsymbol{\nu}}) \\ \tilde{\boldsymbol{\varepsilon}}_v &= \tilde{\boldsymbol{\nu}} - \boldsymbol{\eta} \end{aligned} \quad (26)$$

For a full account of ELBO maximization (or free energy minimization) in active inference, see [26]. Differently from the update rules of predictive coding, we note here additional terms arising from the inferred dynamics. In this way, the model is able to capture the causal relationships between different variables, along with their evolution. Also note that since we are minimizing over (dynamic) paths and non (static) states, an additional term $\mathcal{D}\tilde{\boldsymbol{\mu}}$ is present: this implies trajectory tracking, during which the VFE is minimized only when the belief over the generalized hidden states $\mathcal{D}\tilde{\boldsymbol{\mu}}$ matches its instantaneous trajectory $\dot{\tilde{\boldsymbol{\mu}}}$.

The second assumption made by active inference is that our brains not only perceive (and learn) the external generative process, but also interact with it in order to reach desired states (e.g., in order to survive, one not only must understand which cause leads to an increase or decrease in temperature, but also take actions to live in a narrow range near 37 degrees). The *free energy principle*, which is at the core of active inference, states that all living organisms act to minimize the free energy (or, equivalently, surprise). In fact, in addition to the perceptual inference of predictive coding, the VFE can be minimized by sampling those sensory observations that conform to the prior beliefs, e.g., $\mathbf{a} = \arg \min_{\mathbf{a}} \mathcal{F}$, where \mathbf{a} are the motor commands. This process is typically called *self-evidencing*, which implies that if I believe to find myself in a narrow range of temperatures, minimizing surprise via action will lead to finding places with such temperatures – hence making my beliefs true. One role of the hidden causes is to define the agent’s priors that ensure survival. These priors generated proprioceptive predictions which are suppressed by motor neurons via classical reflex arcs [54]:

$$\dot{\mathbf{a}} = -\partial_{\mathbf{a}} \mathcal{F}_p = -\partial_{\mathbf{a}} \tilde{\mathbf{y}}_p \tilde{\mathbf{\Pi}}_p \tilde{\boldsymbol{\varepsilon}}_p \quad (27)$$

where $\partial_{\mathbf{a}} \tilde{\mathbf{y}}_p$ is an inverse model from observations to action, and $\tilde{\boldsymbol{\varepsilon}}_p = \tilde{\mathbf{y}}_p - \tilde{\mathbf{g}}_p(\tilde{\boldsymbol{\mu}})$ are the generalized proprioceptive prediction errors.

As in predictive coding, we can scale up this generative model to capture the causal relationships of several entities, up to a certain depth [45, 33, 73]. Therefore, the prior becomes the prediction from the layer above, while the observation becomes the likelihood of the layer below:

$$\begin{aligned} \dot{\tilde{\boldsymbol{\mu}}}^{(l)} &= \mathcal{D}\tilde{\boldsymbol{\mu}}^{(l)} + \partial \tilde{\mathbf{g}}^{(l)T} \tilde{\mathbf{\Pi}}_v^{(l)} \tilde{\boldsymbol{\varepsilon}}_v^{(l)} + \partial_\mu \tilde{\mathbf{f}}^{(l)T} \tilde{\mathbf{\Pi}}_x^{(l)} \tilde{\boldsymbol{\varepsilon}}_x^{(l)} - \mathcal{D}^T \tilde{\mathbf{\Pi}}_x^{(l)} \tilde{\boldsymbol{\varepsilon}}_x^{(l)} \\ \dot{\tilde{\boldsymbol{\nu}}}^{(l)} &= \mathcal{D}\tilde{\boldsymbol{\nu}}^{(l)} + \partial_\nu \tilde{\mathbf{f}}^{(l)T} \tilde{\mathbf{\Pi}}_x^{(l)} \tilde{\boldsymbol{\varepsilon}}_x^{(l)} - \tilde{\mathbf{\Pi}}_v^{(l-1)} \tilde{\boldsymbol{\varepsilon}}_v^{(l-1)} \end{aligned} \quad (28)$$

where:

$$\begin{aligned} \tilde{\boldsymbol{\varepsilon}}_x^{(l)} &= \mathcal{D}\tilde{\boldsymbol{\mu}}_x^{(l)} - \tilde{\mathbf{f}}^{(l)}(\tilde{\boldsymbol{\mu}}^{(l)}, \tilde{\boldsymbol{\nu}}^{(l)}) \\ \tilde{\boldsymbol{\varepsilon}}_v^{(l)} &= \tilde{\boldsymbol{\mu}}_v^{(l+1)} - \tilde{\mathbf{g}}^{(l)}(\tilde{\boldsymbol{\mu}}^{(l)}) \end{aligned} \quad (29)$$

and the subscript indicates the index of the level, as before. As clear, the most important role of the hidden causes is to link hierarchical levels. This allows the agent to construct a hierarchy of representations varying at different temporal

scales, critical for realizing richly structured behaviors such as linguistic communication [34] or singing [74]. In this case, the motor commands minimize the generalized prediction errors of the lowest level of the hierarchy.

This continuous formulation of active inference is highly effective for dealing with the dynamicity of realistic environments. However, minimizing the VFE (which is the free energy of the past and present) is unable to perform planning and decision-making in the immediate future. To do this, we construct a discrete generative model with categorical distributions and minimize instead the *Expected Free Energy* (EFE) which, as the name suggests, is the free energy that the agents expect to perceive in the future [75, 26]. This discrete generative model is specular to the continuous model defined above, with the difference that we condition the hidden states over policies π (which in active inference are sequences of discrete actions):

$$p(s, o, \pi) = p(o|s, \pi)p(s|\pi)p(\pi) \quad (30)$$

where s and o are discrete states and outcomes – which do not represent instantaneous trajectories but past, present, and future states as in Hidden Markov Models. Then, the EFE is specifically constructed by considering future states as random variables that need to be inferred:

$$\mathcal{G}_\pi = \mathbb{E}_{q(s, o|\pi)} \left[\ln \frac{q(s|\pi)}{p(s, o|\pi)} \right] \approx \mathbb{E}_{q(s, o|\pi)} \left[\ln \frac{q(s)}{q(s|o, \pi)} \right] - \mathbb{E}_{q(o|\pi)} [\ln p(o|C)] \quad (31)$$

where $q(o|\pi)$ is the recognition distribution that the agent constructs to infer the real posterior of the generative process. Critically, the probability distribution $p(o|C)$ encodes preferred outcomes, acting similar to a prior over the hidden causes in the continuous counterpart. The last two terms are respectively called *epistemic* (uncertainty reducing) and *pragmatic* (goal seeking). In practice, this quantity is used by first factorizing the agent’s generative model as in POMDPs:

$$p(s_{1:T}, o_{1:T}, \pi) = p(s_1) \cdot p(\pi) \cdot \prod_{\tau=1}^T p(o_\tau|s_\tau) \cdot \prod_{\tau=2}^T p(s_\tau|s_{\tau-1}, \pi) \quad (32)$$

Each of these elements can be represented with categorical distributions:

$$\begin{aligned} p(s_1) &= \text{Cat}(\mathbf{D}) & p(o_\tau|s_\tau) &= \text{Cat}(\mathbf{A}) \\ p(\pi) &= \text{Cat}(\mathbf{E}) & p(s_\tau|s_{\tau-1}, \pi) &= \text{Cat}(\mathbf{B}_{\pi, \tau}) \end{aligned} \quad (33)$$

where \mathbf{D} encodes beliefs about the initial state, \mathbf{E} encodes the prior over policies, \mathbf{A} is the likelihood matrix and $\mathbf{B}_{\pi, \tau}$ is the transition matrix. The minimization of EFE in discrete models follows the variational method used by predictive coding and continuous-time active inference; specifically, the use of categorical distribution breaks down the inference of hidden states and policies to a simple local message passing:

$$\begin{aligned} s_{\pi, \tau} &= \sigma(\ln \mathbf{B}_{\pi, \tau-1} s_{\pi, \tau-1} + \ln \mathbf{B}_{\pi, \tau}^T s_{\pi, \tau+1} + \ln \mathbf{A}^T o_\tau) \\ \pi &= \sigma(\ln \mathbf{E} - \mathcal{G}) \\ \mathcal{G}_\pi &\approx \sum_{\tau} \mathbf{A} s_{\pi, \tau} (\ln \mathbf{A} s_{\pi, \tau} - \ln p(o_\tau|C)) - s_{\pi, \tau} \text{diag}(\mathbf{A}^T \ln \mathbf{A}) \end{aligned} \quad (34)$$

For a complete treatment of how the EFE and the approximate posteriors are computed – along with other insightful implications of the free energy principle in discrete models – see [71], while [76] provides a more practical tutorial with basic applications. Here, we note that the update rule for the discrete hidden states at time τ and conditioned over a policy π is a combination of the transition messages coming from the previous and next discrete time steps, and a likelihood message coming from the discrete outcome. This combination is passed to a softmax function in order to get a proper probability. Instead, the optimal policy π is found by a combination of a policy prior and the EFE, where the latter is a composition of epistemic and pragmatic behaviors. Policy inference can be refined by computing the EFE of several steps ahead in the future – a process called *sophisticated inference*. At each discrete step τ , the agents selects the most likely action u under all policies, i.e., $u_t = \arg \max_u \pi \cdot [U_{\pi, t} = u]$.

As before, we can construct a hierarchical structure able to express more and more invariant representations of hidden states [77]. In discrete state-space, links between hierarchical levels are usually done between hidden states via the matrix \mathbf{D} – although some formulations allow the hidden states of a level to condition the policies of the subordinate

levels. The update rules for this hierarchical alternative become:

$$\begin{aligned} \mathbf{s}_{\pi,\tau}^{(l)} &= \sigma(\ln \mathbf{B}_{\pi,\tau-1}^{(l)} \mathbf{s}_{\pi,\tau-1}^{(l)} + \ln \mathbf{B}_{\pi,\tau}^{(l)T} \mathbf{s}_{\pi,\tau+1}^{(l)} + \ln \mathbf{A}^{(l)T} \mathbf{o}_{\tau}^{(l)} + \ln \mathbf{D}^{(l+1)T} \mathbf{s}_1^{(l+1)}) \\ \boldsymbol{\pi}^{(l)} &= \sigma(\ln \mathbf{E}^{(l)} - \mathcal{G}^{(l)}) \\ \mathcal{G}_{\pi}^{(l)} &\approx \sum_{\tau} \mathbf{A}^{(l)} \mathbf{s}_{\pi,\tau}^{(l)} (\ln \mathbf{A}^{(l)} \mathbf{s}_{\pi,\tau}^{(l)} - \ln p(\mathbf{o}_{\tau}^{(l)} | \mathbf{C})) - \mathbf{s}_{\pi,\tau}^{(l)} \text{diag}(\mathbf{A}^{(l)T} \ln \mathbf{A}^{(l)}) \end{aligned} \quad (35)$$

This implies that each level takes abstract actions to minimize its EFE, only depending on the levels immediately below and above.

C Bayesian model comparison

Bayesian model comparison is a technique used to compare a posterior over some data with a few simple hypotheses known a-priori [51]. Consider a generative model $p(\boldsymbol{\theta}, \mathbf{y})$ with parameters $\boldsymbol{\theta}$ and data \mathbf{y} :

$$p(\boldsymbol{\theta}, \mathbf{y}) = p(\mathbf{y} | \boldsymbol{\theta}) p(\boldsymbol{\theta}) \quad (36)$$

We introduce additional distributions $p(\mathbf{y}, \boldsymbol{\theta} | m)$ which are reduced versions of the first model if the likelihood of some data is the same under both models and the only difference rests upon the specification of the priors $p(\boldsymbol{\theta} | m)$. We can express the posterior of the reduced models in terms of the posterior of the full model and the ratios of the priors and the evidence:

$$p(\boldsymbol{\theta} | \mathbf{y}, m) = p(\boldsymbol{\theta} | \mathbf{y}) \frac{p(\boldsymbol{\theta} | m) p(\mathbf{y})}{p(\boldsymbol{\theta}) p(\mathbf{y} | m)} \quad (37)$$

The procedure for computing the reduced posteriors is the following: first, we integrate over the parameters to obtain the evidence ratio of the two models:

$$p(\mathbf{y} | m) = p(\mathbf{y}) \int p(\boldsymbol{\theta} | \mathbf{y}) \frac{p(\boldsymbol{\theta} | m)}{p(\boldsymbol{\theta})} d\boldsymbol{\theta} \quad (38)$$

Then, we define an approximate posterior $q(\boldsymbol{\theta})$ and we compute the reduced free energies of each model m :

$$\mathcal{F}[p(\boldsymbol{\theta} | m)] \approx \mathcal{F}[p(\boldsymbol{\theta})] + \ln \mathbb{E}_q \left[\frac{p(\boldsymbol{\theta} | m)}{p(\boldsymbol{\theta})} \right] \quad (39)$$

This VFE acts as a hint to how well the reduced representation explains the full model. Similarly, the approximate posterior of the reduced model can be written in terms of the posterior of the full model:

$$\ln q(\boldsymbol{\theta} | m) = \ln q(\boldsymbol{\theta}) + \ln \frac{p(\boldsymbol{\theta} | m)}{p(\boldsymbol{\theta})} - \ln \mathbb{E}_q \left[\frac{p(\boldsymbol{\theta} | m)}{p(\boldsymbol{\theta})} \right] \quad (40)$$

The Laplace approximation [78] leads to a simple form of the approximate posterior and the reduced free energy. Assuming the following Gaussian distributions:

$$\begin{aligned} p(\boldsymbol{\theta}) &= \mathcal{N}(\boldsymbol{\eta}, \boldsymbol{\Sigma}) & q(\boldsymbol{\theta}) &= \mathcal{N}(\boldsymbol{\mu}, \mathbf{C}) \\ p(\boldsymbol{\theta} | m) &= \mathcal{N}(\boldsymbol{\eta}_m, \boldsymbol{\Sigma}_m) & q(\boldsymbol{\theta} | m) &= \mathcal{N}(\boldsymbol{\mu}_m, \mathbf{C}_m) \end{aligned} \quad (41)$$

The reduced free energy turns to:

$$\begin{aligned} \mathcal{F}[p(\boldsymbol{\theta} | m)] &\approx \frac{1}{2} \ln |\boldsymbol{\Pi}_m \mathbf{P} \mathbf{C}_m \boldsymbol{\Sigma}| \\ &\quad - \frac{1}{2} (\boldsymbol{\mu}^T \mathbf{P} \boldsymbol{\mu} - \boldsymbol{\mu}_m^T \mathbf{P}_m \boldsymbol{\mu}_m - \boldsymbol{\eta}^T \boldsymbol{\Pi} \boldsymbol{\eta} + \boldsymbol{\eta}_m^T \boldsymbol{\Pi}_m \boldsymbol{\eta}_m) \end{aligned} \quad (42)$$

expressed in terms of precision of priors \mathbf{P} and posteriors $\boldsymbol{\Pi}$. The reduced posterior mean and precision are computed via Equation 40:

$$\begin{aligned} \boldsymbol{\mu}_m &= \mathbf{C}_m (\mathbf{P} \boldsymbol{\mu} - \boldsymbol{\Pi} \boldsymbol{\eta} + \boldsymbol{\Pi}_m \boldsymbol{\eta}_m) \\ \mathbf{P}_m &= \mathbf{P} - \boldsymbol{\Pi} + \boldsymbol{\Pi}_m \end{aligned} \quad (43)$$

In this way, two different hypotheses i and j can be compared in order to infer which one is the most likely to have generated the observed data; this comparison has the form of a log-Bayes factor $\mathcal{F}[p(\theta|i)] - \mathcal{F}[p(\theta|j)]$. For a more detailed treatment of Bayesian model comparison (and in particular under the Laplace approximation), see [51, 50].

D Implementation details

The agent's sensory modalities are: (i) a proprioceptive observation \mathbf{y}_p for the arm's joint angles; (ii) a visual observation \mathbf{y}_v encoding the Cartesian positions of every link of the arm, both extremities of the tool, and the ball; (iii) a discrete tactile observation \mathbf{o}_t signaling whether or not the target is grasped.

We decompose intrinsic and extrinsic hidden states of every IE module into three components, corresponding to the arm, the tool, and the ball. Hence:

$$\begin{aligned}\mathbf{x}_i^{(i)} &= \begin{bmatrix} \mathbf{x}_{i,a}^{(i)} & \mathbf{x}_{i,t}^{(i)} & \mathbf{x}_{i,b}^{(i)} \end{bmatrix} \\ \mathbf{x}_e^{(i)} &= \begin{bmatrix} \mathbf{x}_{e,a}^{(i)} & \mathbf{x}_{e,t}^{(i)} & \mathbf{x}_{e,b}^{(i)} \end{bmatrix}\end{aligned}\tag{44}$$

For each entity, the intrinsic hidden states encode pairs of joint angles and segment lengths, e.g., $\mathbf{x}_{i,a}^{(i)} = [\theta_a^{(i)}, l_a^{(i)}]$ while the extrinsic reference frame is expressed in terms of the position of a segment's extremity and its absolute orientation, e.g., $\mathbf{x}_{e,a}^{(i)} = [p_{a,x}^{(i)}, p_{a,y}^{(i)}, \phi_a^{(i)}]$. The likelihood function \mathbf{g}_e of Equation 12 computes extrinsic predictions independently for each entity:

$$\mathbf{g}_e(\mathbf{x}_i^{(i)}, \mathbf{x}_e^{(i-1)}) = \begin{bmatrix} \mathbf{T}(\mathbf{x}_{i,a}^{(i)}, \mathbf{x}_{e,a}^{(i-1)}) & \mathbf{T}(\mathbf{x}_{i,t}^{(i)}, \mathbf{x}_{e,t}^{(i-1)}) & \mathbf{T}(\mathbf{x}_{i,b}^{(i)}, \mathbf{x}_{e,b}^{(i-1)}) \end{bmatrix}\tag{45}$$

Here, the function $\mathbf{T}(\mathbf{x}_i, \mathbf{x}_e)$ reduces to a simple roto-translation:

$$\mathbf{T}(\mathbf{x}_i, \mathbf{x}_e) = \begin{bmatrix} p_x + l c_{\theta, \phi} \\ p_y + l s_{\theta, \phi} \\ \phi + \theta \end{bmatrix}\tag{46}$$

where $\mathbf{x}_i = [\theta, l]$, $\mathbf{x}_e = [p_x, p_y, \phi]$, and we used a compact notation to indicate the sine and cosine of the sum of two angles, i.e., $c_{\theta, \phi} = \cos(\theta) \cos(\phi) - \sin(\theta) \sin(\phi)$. Each level then computes proprioceptive and visual predictions through likelihood functions \mathbf{g}_p and \mathbf{g}_v , which in this case are simple mappings that extract the joint angles of the arm and the Cartesian positions of the objects from the intrinsic and extrinsic hidden states, respectively:

$$\begin{aligned}\mathbf{g}_p(\mathbf{x}_i^{(i)}) &= \theta_a^{(i)} \\ \mathbf{g}_v(\mathbf{x}_e^{(i)}) &= \begin{bmatrix} p_{a,x}^{(i)} & p_{t,x}^{(i)} & p_{b,x}^{(i)} \\ p_{a,y}^{(i)} & p_{t,y}^{(i)} & p_{b,y}^{(i)} \end{bmatrix}\end{aligned}\tag{47}$$

Reaching the tool's origin with the end effector may be achieved through a function (related to an agent's *intention* [79, 56]) that sets the first component of the corresponding extrinsic hidden states equal to the second one:

$$\mathbf{i}_{e,t}^{(4)}(\mathbf{x}_e^{(4)}) = \begin{bmatrix} \mathbf{x}_{e,t}^{(4)} & \mathbf{x}_{e,t}^{(4)} & \mathbf{x}_{e,b}^{(4)} \end{bmatrix}\tag{48}$$

Then, we define a reduced dynamics function by subtracting the current hidden states from this intention:

$$\mathbf{f}_{e,t}^{(4)}(\mathbf{x}_e^{(4)}) = \mathbf{i}_{e,t}^{(4)}(\mathbf{x}_e^{(4)}) - \mathbf{x}_e^{(4)} = \begin{bmatrix} \mathbf{x}_{e,t}^{(4)} - \mathbf{x}_{e,a}^{(4)} & \mathbf{0} & \mathbf{0} \end{bmatrix}\tag{49}$$

Note the decomposition into separate attractors. A non-zero velocity for the first component expresses the agent's desire to move the arm, while a zero velocity for the other two components means that the agent does not intend to manipulate them during the first step of the task. Further, since a potential kinematic configuration for the tool is already at the agent's disposal, in order to speed up the movement similar intentions can be imposed at every hierarchical level, both in intrinsic and extrinsic reference frames. At this point, all that remains is to reach the ball with the tool's extremity. But how is this possible if the arm's belief – the only one generating proprioceptive predictions – does not encode the

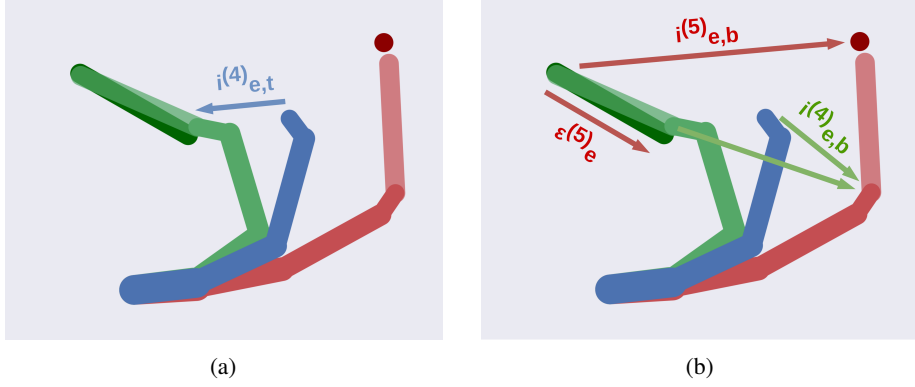


Figure 8: Representation of the intentions active during the two steps. (a) The end effector is pulled toward the belief about the tool's origin through $i_{e,t}^{(4)}$. (b) The last level of the tool component is pulled toward the ball through intention $i_{e,b}^{(5)}$. This generates an extrinsic prediction error $\epsilon_e^{(5)}$ that steers the previous level of the tool component. Concurrently, a second intention $i_{e,b}^{(4)}$ also pulls both arm and tool components of the end effector level.

virtual level? First, we link the virtual extrinsic hidden states of the tool's extremity:

$$\mathbf{i}_{e,b}^{(5)}(\mathbf{x}_e^{(5)}) = \begin{bmatrix} \mathbf{x}_{e,b}^{(5)} & \mathbf{x}_{e,b}^{(5)} \end{bmatrix} \quad (50)$$

Then, we define an intention that sets the first two components of the end effector's extrinsic hidden states equal to the third one:

$$\mathbf{i}_{e,b}^{(4)}(\mathbf{x}_e^{(4)}) = \begin{bmatrix} \mathbf{x}_{e,b}^{(4)} & \mathbf{x}_{e,b}^{(4)} & \mathbf{x}_{e,b}^{(4)} \end{bmatrix} \quad (51)$$

Maintaining these two intentions at the same time eventually drives the end effector into a suitable position that makes the tool's extremity touch the ball. A representation of the relations between such intentions is displayed in Figure 8.

Now, we define the hidden causes of the last two levels:

$$\begin{aligned} \mathbf{v}_e^{(4)} &= \begin{bmatrix} v_s^{(4)} & v_t^{(4)} & v_b^{(4)} \end{bmatrix} \\ \mathbf{v}_e^{(5)} &= \begin{bmatrix} v_s^{(5)} & v_b^{(5)} \end{bmatrix} \end{aligned} \quad (52)$$

where the subscripts s , t , and b indicate the agent's intentions to maintain the current state of the world, reach the tool, and reach the ball, respectively. Note that the first hidden cause, related to the following intentions:

$$\mathbf{i}_{e,s}^{(4)}(\mathbf{x}_e^{(4)}) = \mathbf{x}_e^{(4)} \quad \mathbf{i}_{e,s}^{(5)}(\mathbf{x}_e^{(5)}) = \mathbf{x}_e^{(5)} \quad (53)$$

are needed to ensure that $\mathbf{v}_e^{(4)}$ and $\mathbf{v}_e^{(5)}$ encode proper categorical distributions when the discrete model is in the initial state. The average trajectory is then found by weighting the reduced dynamics functions of the defined intentions with the corresponding hidden causes. Hence, having indicated with $\boldsymbol{\mu}_e^{(4)}$ the *belief* over the hidden states of the end effector level:

$$\boldsymbol{\eta}_{x,e}^{(4)} = v_s^{(4)} \mathbf{f}_{e,s}^{(4)}(\boldsymbol{\mu}_e^{(4)}) + v_t^{(4)} \mathbf{f}_{e,t}^{(4)}(\boldsymbol{\mu}_e^{(4)}) + v_b^{(4)} \mathbf{f}_{e,b}^{(4)}(\boldsymbol{\mu}_e^{(4)}) \quad (54)$$

This belief is then updated according to:

$$\begin{aligned} \dot{\boldsymbol{\mu}}_e^{(4)} &= \boldsymbol{\mu}_e^{(4)} - \boldsymbol{\pi}_e^{(4)} \boldsymbol{\varepsilon}_e^{(4)} + \partial \mathbf{g}_e^T \boldsymbol{\pi}_e^{(5)} \boldsymbol{\varepsilon}_e^{(5)} + \partial \mathbf{g}_v^T \boldsymbol{\pi}_v^{(4)} \boldsymbol{\varepsilon}_v^{(4)} + \partial \boldsymbol{\eta}_{x,e}^{(4)T} \boldsymbol{\pi}_{x,e}^{(4)} \boldsymbol{\varepsilon}_{x,e}^{(4)} \\ \dot{\boldsymbol{\mu}}_e^{(4)} &= -\boldsymbol{\pi}_{x,e}^{(4)} \boldsymbol{\varepsilon}_{x,e}^{(4)} \end{aligned} \quad (55)$$

In short, the 0th-order is subject to: (i) a force proportional to its predicted velocity; (ii) an extrinsic prediction error coming from the elbow, i.e., $\boldsymbol{\varepsilon}_e^{(5)} = \boldsymbol{\mu}_e^{(5)} - \mathbf{g}_e(\boldsymbol{\mu}_i^{(5)}, \boldsymbol{\mu}_e^{(4)})$; (iii) a backward extrinsic prediction error coming from the

virtual level; (iv) a visual prediction error, i.e., $\varepsilon_v^{(4)} = \mathbf{y}_v^{(4)} - \boldsymbol{\mu}_e^{(4)}$; (v) a backward dynamics error encoding the agent's intentions, i.e., i.e., $\varepsilon_{x,e}^{(4)} = \boldsymbol{\mu}_e'^{(4)} - \boldsymbol{\eta}_{x,e}^{(4)}$.

The actions \mathbf{a} are instead computed by minimizing the proprioceptive prediction errors:

$$\dot{\mathbf{a}} = -\partial_a \mathbf{g}_p^T \boldsymbol{\pi}_p \varepsilon_p \quad (56)$$

where $\partial_a \mathbf{g}_p$ performs an inverse dynamics from the proprioceptive predictions to the actions.

As concerns the discrete model, its hidden states \mathbf{s} can express: (i) whether the agent is at the tool position, at the ball position, or none of the two; (ii) whether the agent has grasped or not the tool. These two factors combine in 6 process states in total. The first factor generates predictions for the extrinsic hidden causes of the hybrid units through likelihood matrices, i.e., $\mathbf{o}_e^{(4)} = \mathbf{A}_e^{(4)} \mathbf{s}$ and $\mathbf{o}_e^{(5)} = \mathbf{A}_e^{(5)} \mathbf{s}$. This allows the agent to synchronize the behavior of both the tool and end effector; similarly, additional likelihood matrices can be defined to impose intentions for the intrinsic hidden states or at different levels of the hierarchy. The second factor returns a discrete tactile prediction, i.e., $\mathbf{o}_t = \mathbf{A}_t \mathbf{s}$.

Finally, we define a discrete action for each agent's intention, and a transition matrix \mathbf{B} such that the ball can be reached only when the tool has been grasped. The bottom-up messages from the hybrid units are updated by comparing high-level expectations and low-level evidences:

$$\begin{aligned} \mathbf{v}_e^{(4)} &= \sigma(-\mathbf{E}_e^{(4)}) = \sigma(\ln \mathbf{A}_e^{(4)} \mathbf{s} + \mathbf{l}_e^{(4)}) \\ \mathbf{v}_e^{(5)} &= \sigma(-\mathbf{E}_e^{(5)}) = \sigma(\ln \mathbf{A}_e^{(5)} \mathbf{s} + \mathbf{l}_e^{(5)}) \end{aligned} \quad (57)$$

where $\mathbf{l}_e^{(4)}$ and $\mathbf{l}_e^{(5)}$ are the bottom-up messages that accumulate continuous log evidence over some time T . The discrete hidden states at time τ are then inferred by combining such messages with the discrete observation and the hidden states at time $\tau - 1$:

$$\mathbf{s}_{\pi,\tau} = \sigma(\ln \mathbf{B}_{\pi,\tau-1} \mathbf{s}_{\tau-1} + \ln \mathbf{A}_e^{(4)T} \mathbf{v}_{e,\tau}^{(4)} + \ln \mathbf{A}_e^{(5)T} \mathbf{v}_{e,\tau}^{(5)} + \ln \mathbf{A}_t^T \mathbf{o}_t) \quad (58)$$

If we assume for simplicity that the agent's preferences are encoded in a tensor \mathbf{C} in terms of expected states, the expected free energy breaks down to:

$$\mathcal{G}_\pi \approx \sum_{\tau} \mathbf{s}_{\pi,\tau} (\ln \mathbf{s}_{\pi,\tau} - \mathbf{C}_\tau) \quad (59)$$

where:

$$\mathbf{C}_\tau = \ln p(\mathbf{s}_\tau | \mathbf{C}) \quad (60)$$

Computing the softmax of the expected free energy returns the posterior probability over the policies π , which are used to infer the new discrete hidden states at time $\tau + 1$.

E Algorithms

Algorithm 1 Compute expected free energy

Input:

length of policies N_p
discrete hidden states s
policies π
transition matrix B
preference C

Output:

expected free energy \mathcal{G}

```

 $\mathcal{G} \leftarrow 0$ 
for each policy  $\pi_\pi$  do
     $s_{\pi,\tau} \leftarrow s$ 
    for  $\tau = 0$  to  $N_p$  do
         $s_{\pi,\tau} \leftarrow B_{\pi,\tau} s_{\pi,\tau}$ 
         $\mathcal{G}_\pi \leftarrow \mathcal{G}_\pi + s_{\pi,\tau} (\ln s_{\pi,\tau} - C)$ 
    end for
end for

```

Algorithm 2 Accumulate log evidence

Input:

mean of full prior η
mean of reduced priors η_m
mean of full posterior μ
precision of full prior π
precision of reduced priors π_m
precision of full posterior p
log evidences L_m

Output:

log evidences L_m

```

for each reduced model  $m$  do
     $p_m \leftarrow p - \pi + \pi_m$ 
     $\mu_m \leftarrow p_m^{-1} (p\mu - \pi\eta + \pi_m\eta_m)$ 
     $\mathcal{L}_m \leftarrow \mathcal{L}_m + (\mu_m^T p_m \mu_m - \eta_m^T \pi_m \eta_m - \mu^T p \mu + \eta^T \pi \eta) / 2$ 
end for

```

Algorithm 3 Active inference with hierarchical hybrid models

Input:

- continuous time T
- discrete time \mathcal{T}
- intrinsic units $\mathcal{U}_i^{(i,j)}$
- extrinsic units $\mathcal{U}_e^{(i,j)}$
- inverse dynamics $\partial_a g_p$
- proprioceptive precisions π_p
- learning rate Δ_t , action a

for $t = 0$ to T **do**

- Get observations
- if** $t \bmod \mathcal{T} = 0$ **then**

 - Update discrete model via Algorithm 4

- end if**
- for** each unit $\mathcal{U}_i^{(i,j)}$ and $\mathcal{U}_e^{(i,j)}$ **do**

 - Update intrinsic unit via Algorithm 5
 - Update extrinsic unit via Algorithm 6

- end for**
- Get proprioceptive prediction errors ε_p from intrinsic units
- $\dot{a} \leftarrow -\partial_a g_p^T \pi_p \varepsilon_p$
- $a \leftarrow a + \Delta_t \dot{a}$
- Take action a

end for

Algorithm 4 Update discrete model at time τ

Input:

- discrete hidden states s
- policies π
- likelihood matrices $\mathbf{A}^{(i,j)}$
- transition matrix B
- prior D
- accumulated log evidences $l^{(i,j)}$

Output:

- accumulated log evidences $l^{(i,j)}$
- discrete hidden causes $v^{(i,j)}$

for each unit $\mathcal{U}^{(i,j)}$ **do**

- $\sigma^{(i,j)} \leftarrow \sigma(\ln \mathbf{A}^{(i,j)} s + l^{(i,j)})$

end for

- $s \leftarrow \sigma(\ln D + \sum_{i,j} \ln \mathbf{A}^{(i,j)T} \sigma^{(i,j)})$
- Compute expected free energy \mathcal{G} via Algorithm 1
- $\pi \leftarrow \sigma(-\mathcal{G})$
- $D \leftarrow \sum_{\pi} \pi_{\pi,0} B_{\pi,0} s$
- for** each unit $\mathcal{U}^{(i,j)}$ **do**

 - $v^{(i,j)} \leftarrow \mathbf{A}^{(i,j)} D$
 - $l^{(i,j)} \leftarrow 0$

end for

Algorithm 5 Update intrinsic unit

Input:

intrinsic belief over hidden states $\tilde{\mu}$
 intrinsic (discrete) hidden causes v
 extrinsic gradient $\partial g_e^T \pi_e \varepsilon_e$
 proprioceptive observation y_p
 dynamics (reduced) functions f_m
 proprioceptive likelihood g_p
 proprioceptive precision π_p
 dynamics precision π_x
 learning rate Δ_t

Output:

intrinsic belief over hidden states μ
 proprioceptive prediction error ε_p

$$\begin{aligned} \eta'_x &\leftarrow \sum_m v_m f_m(\mu) \\ \varepsilon_x &\leftarrow \mu' - \eta'_x \\ \varepsilon_p &\leftarrow y_p - g_p(\mu) \\ \text{Accumulate log evidence via Algorithm 2} \\ \dot{\mu} &\leftarrow \mu' + \partial g_e^T \pi_e \varepsilon_e + \partial g_p^T \pi_p \varepsilon_p + \partial \eta'_x^T \pi_x \varepsilon_x \\ \dot{\mu}' &\leftarrow -\pi_x \varepsilon_x \\ \tilde{\mu} &\leftarrow \tilde{\mu} + \Delta_t \dot{\mu} \end{aligned}$$

Algorithm 6 Update extrinsic unit

Input:

extrinsic belief over hidden states $\tilde{\mu}$
 extrinsic (discrete) hidden causes v
 prior likelihood (i.e., extrinsic likelihood from previous level) g_η
 intrinsic prior (from same level) η_i
 extrinsic prior (from previous level) η_e
 prior precision π_η
 extrinsic gradients (from next level) $\partial g_e^{(j)T} \pi_e^{(j)} \varepsilon_e^{(j)}$
 visual observation y_v
 dynamics (reduced) functions f_m
 visual likelihood g_v
 visual precision π_v
 dynamics precision π_x
 learning rate Δ_t

Output:

extrinsic belief over hidden states μ
 gradient wrt intrinsic prior $\partial_{\eta_i} g_\eta^T \pi_\eta \varepsilon_\eta$
 gradient wrt extrinsic prior $\partial_{\eta_e} g_\eta^T \pi_\eta \varepsilon_\eta$

$$\begin{aligned} \eta'_x &\leftarrow \sum_m v_m f_m(\mu) \\ \varepsilon_\eta &\leftarrow \mu - g_\eta(\eta_i, \eta_\eta) \\ \varepsilon_x &\leftarrow \mu' - \eta'_x \\ \varepsilon_v &\leftarrow y_v - g_v(\mu) \\ \text{Accumulate log evidence via Algorithm 2} \\ \dot{\mu} &\leftarrow \mu' - \pi_\eta \varepsilon_\eta + \sum_j \partial g_e^{(j)T} \pi_e^{(j)} \varepsilon_e^{(j)} + \partial g_v^T \pi_v \varepsilon_v + \partial \eta'_x^T \pi_x \varepsilon_x \\ \dot{\mu}' &\leftarrow -\pi_x \varepsilon_x \\ \tilde{\mu} &\leftarrow \tilde{\mu} + \Delta_t \dot{\mu} \end{aligned}$$
